Pre-existing antibodies targeting a linear epitope on SARS-CoV-2 S2 cross-reacted with commensal gut bacteria and shaped vaccine induced immunity

Liqiu Jia[1, §], Shufeng Weng[2, §], Jing Wu[1, §], Xiangxiang Tian[3, 4], Yifan Zhang[3, 4], Xuyang Wang[1], Jing Wang[3, 5], Dongmei Yan[5], Wanhai Wang[4], Zhaoqin Zhu[3, #], Chao Qiu[6, #], Wenhong Zhang[1, 2, 7, 8, #], Ying Xu[2, #], Yanmin Wan[1, 2, 9, #]

[1] Department of Infectious Diseases, National Medical Center for Infectious Diseases, Shanghai Key Laboratory of Infectious Diseases and Biosafety Emergency Response, Huashan Hospital, Shanghai Medical College, Fudan University, Shanghai, China;
[2] State Key Laboratory of Genetic Engineering, Institute of Genetics, School of Life Science, Fudan University, Shanghai, China;
[3] Department of laboratory medicine, Shanghai Public Health Clinical Center, Shanghai, China;
[4] Clinical Laboratory, The First Affiliated Hospital of Zhengzhou University, Key Laboratory of Laboratory Medicine of Henan Province, Zhengzhou, Henan, P.R. China;
[5] Department of Immunology, School of Basic Medical, Jiamusi University, Jiamusi, Heilongjiang Province, China;
[6] Institutes of biomedical sciences & Shanghai Key Laboratory of Medical Epigenetics, Fudan University, Shanghai, China;
[7] National Clinical Research Center for Aging and Medicine, Huashan Hospital, Shanghai Medical College, Fudan University, Shanghai, China;
[8] Key Laboratory of Medical Molecular Virology (MOE/MOH) and Institutes of Biomedical Sciences, Shanghai Medical College, Fudan University, Shanghai, China.
[9] Department of radiology, Shanghai Public Health Clinical Center, Shanghai, China
[§] These authors contribute equally to this work.
[#] Correspondence should be addressed to: Zhaoqin Zhu, zhaoqinzhu@163.com; Chao Qiu, qiuchao@fudan.edu.cn; Wenhong Zhang, zhangwenhong@fudan.edu.cn; Ying Xu, yingxu2520@fudan.edu.cn; Yanmin Wan, yanmin_wan@fudan.edu.cn

Running title: SARS-CoV-2 antibody cross-reacts with gut bacteria

Word count: Abstract, 214; main text, 6208

Abstract

The origins of pre-existing SARS-CoV-2 cross-reactive antibodies and their potential impacts on vaccine efficacy have not been fully clarified. In this study, we demonstrated that S2 was the prevailing target of the pre-existing S protein cross-reactive antibodies in both healthy human and SPF mice. A dominant antibody epitope was identified on the connector domain of S2 (1147-SFKEELDKYFKNHT-1160, P144), which could be recognized by pre-existing antibodies in both human and mouse. Through metagenomic sequencing and fecal bacteria transplant, we proved that the generation of S2 cross-reactive antibodies was associated with commensal gut bacteria. Furthermore, six P144 specific monoclonal antibodies were isolated from mouse and proved to cross-react with commensal gut bacteria collected from both human and mouse. Mice with high levels of pre-existing S2 cross-reactive antibodies mounted higher S protein specific binding antibodies, especially against S2, after being immunized with a candidate COVID-19 DNA vaccine. Similarly, we found that levels of pre-existing antibodies against both S2 and P144 correlated positively with RBD specific binding antibody titers after two doses of inactivated SARS-CoV-2 vaccination in human. Taken together, our findings revealed that the pre-existing cross-reactive antibodies against SARS-CoV-2 spike protein could be induced by commensal gut bacteria and suggested that these pre-existing cross-reactive antibodies could facilitate the induction of S protein specific antibody responses after vaccination.

Key words: Cross-reactive antibody, SARS-CoV-2, Spike protein, commensal gut bacteria, vaccine immunogenicity

Introduction

Antibodies are vital components of the immune system that mediate protection against infections (1). When confronting infections, the actual role of pre-existing antibody depends on the following features (2): High titers of broadly neutralizing antibodies can protect the host against infection. While, when the pre-existing antibodies are non-neutralizing or with only a narrow neutralizing spectrum, hosts may not be sterilely protected or only be protected against specific serotypes of viruses. In addition to defending hosts against infections, pre-existing antibodies can also impact host immune responses upon infection or vaccination (3-5), which is best exemplified by the observations showing that pre-existing antibodies shaped the recall immune responses against influenza (6, 7).

For most occasions, pre-existing antibodies in adults derive from previous infection or vaccination except some “naturally” produced, poly-reactive antibodies (2, 8). When encountering a newly emerged or mutated virus, cross-reactive antibodies induced by previously occurred, phylogenetically closely related viruses constitute the main body of the pre-existing cross-reactive antibodies. The effect of this kind of pre-existing antibodies has been extensively investigated especially for infections of influenza (3, 7, 9) and flaviviruses (10-12). Of note, previous infection by phylogenetically similar viruses is not the sole source of pre-existing cross-reactive antibodies, as it has been clearly clarified that pre-existing antibodies against HIV-1 gp41 may stem from exposures to certain commensal gut bacteria (13-15). Besides, autoimmune diseases caused by cross-reactivities between microbial and self-antigens also implied that commensal gut bacteria represent important sources of cross-reactive antibodies (16-19).

Pre-existing antibodies against SARS-CoV-2 have also been observed in uninfected healthy individuals, which are speculated to be engendered by previous exposures to human common cold coronaviruses (20-26) or SARS-CoV (27-29). Meanwhile, sequence analyses (30) and a clinical observation (31) suggest that pre-existing SARS-CoV-2 antibodies might be engendered by common human pathogens and childhood vaccination. Although these two explanations are not mutually exclusive, they both need more experimental evidence to support.

In this study, we found that higher levels of SARS-CoV-2 S2 protein specific

101 antibodies existed in both healthy human and naïve SPF mice. To track the
102 potential origins of these pre-existing cross-reactive antibodies, we mapped
103 and located a dominant linear antibody epitope on S2, which could be
104 recognized by pre-existing antibodies from both healthy human and naïve SPF
105 mice. Monoclonal antibodies against this linear epitope were isolated from
106 naïve SPF mice and proved to cross-react with commensal gut bacteria
107 collected from both healthy human and naïve SPF mouse. Moreover, despite
108 having been discussed iteratively (32, 33), the influences of pre-existing
109 cross-reactive immunities on COVID-19 responses have not been clarified.
110 Here we showed that high levels of pre-existing antibodies did not impair the
111 immunogenicity of a candidate DNA vaccine encoding SARS-CoV-2 spike
112 protein. On the contrary, mice with high levels of pre-existing antibodies
113 mounted stronger S2 specific binding antibody responses compared with mice
114 with low levels of pre-existing antibodies after immunization with a candidate
115 DNA vaccine. Meanwhile, S1 specific T cell and binding antibody responses
116 also tended to be stronger in mice with high levels of pre-existing antibodies,
117 although no statistical significance was reached.
118

119 **Results**

120 **Pre-existing antibodies recognizing a dominant linear epitope on**
121 **SARS-CoV-2 S2 protein were detected in both human and mice**

122 Pre-existing antibodies cross-react with SARS-CoV-2 S protein have been
123 found in uninfected individuals by multiple previous studies (22, 25, 26, 34). It
124 was postulated that the pre-existing immunities against SARS-CoV-2 might be
125 induced by previous exposure to seasonal human coronaviruses (22, 30, 32,
126 33, 35). However, contradictive evidence suggested that human common cold
127 coronavirus infection did not necessarily induce antibodies cross-reactive with
128 SARS-CoV-2 spike protein (28, 36, 37). In addition to this hypothesis, an
129 alternative explanation suggested that the cross-reactive immunities to
130 SARS-CoV-2 might derive from other common human pathogens and
131 vaccines (38).

132 To track the origins of the pre-existing cross-reactive antibodies to
133 SARS-CoV-2 spike protein, in this study, we first measured the levels of
134 pre-existing S protein specific antibodies in healthy human individuals and
135 SPF mice. Our data showed that the cross-reactive antibody responses

136 against S2 were significantly stronger than those against S1 in plasma
137 samples of healthy human collected both pre (2016 cohort) and post (2020
138 cohort) the outbreak of COVID-19 pandemic (Fig.1A and 1B). More strikingly,
139 our data showed that binding antibodies targeting S2 could also be detected in
140 two strains of naïve SPF mice (Fig. 1C and 1D). And this finding was further
141 confirmed by Western-blotting (WB) assays, which showed that mouse sera
142 with high ELISA-detected OD values (Fig. 2A) bound specifically with purified
143 S2 while not S1 (Fig. 2B). Quite interestingly, the WB results indicated that
144 cross-reactive antibodies against S2 also existed in the serum of a mouse
145 (#487) with no detectable binding signal in the S2 ELISA assay (Fig. 2A and
146 2B). We next performed linear antibody epitope mapping using an in-house
147 developed method of peptide competition ELISA. Our data showed that a
148 single peptide (P144, aa1145-aa1162, 18 mer) accounted for most of the
149 observed pre-existing antibody responses towards S2 in mice (Supplementary
150 Figure 1). Via employing a series of truncated peptides based on P144, we
151 determined the minimal range of this epitope
152 (1147-SFKEELDKYFKNHT-1160), which locates on the connector domain
153 (adjacent to the N-terminal of HR2 domain) (Fig. 2C). We also proved that
154 antibodies recognizing this epitope widely existed in both healthy human and
155 naïve SPF mice using the competitive ELISA assay (Fig.3).
156
157 **The P144 specific antibody responses were engendered by exposures to**
158 **certain commensal gut bacteria**
159 To explore the potential origins of the pre-existed P144 specific antibodies, we
160 first performed phylogenetic analyses among SARS-CoV-2 and other human
161 coronaviruses. The results showed that the aa sequence of P144 was highly
162 conserved among SARS-CoV-2 variants and SARS-CoV, while the similarities
163 between P144 and MERS-CoV or seasonal human coronaviruses were
164 relatively low, especially within the range of predicted antibody binding epitope
165 (boxed fragment) (Supplementary Figure 2). The possibility of coronavirus
166 infection in our SPF-mouse colonies was excluded by serum screening tests
167 using commercialized mouse hepatitis virus (MHV) antigen and antibody
168 detection kits (Data not shown).
169 Subsequently, to investigate whether environmental factors contribute to the
170 induction of these S2 cross-reactive antibodies, we compared the levels of

171 pre-existing S2 binding antibodies between mice housed in SPF condition and
172 mice maintained in a sterile isolation pack. Our data showed that the levels of
173 pre-existing S2 binding antibodies were significantly higher in SPF mice
174 (Figure 4A). Through metagenomic sequencing, we further demonstrated that
175 the compositions of commensal gut bacteria were significantly different
176 between mice housed in SPF condition and mice maintained in the sterile
177 isolation pack (Supplementary Figure 3A). The abundance of bacteroidaceae,
178 prevotellaceace and parabacteroides increased significantly in the commensal
179 gut bacteria of SPF mice (Figure 4B). Moreover, flowcytometry assays
180 indicated that the frequencies of S2 specific B cells ($CD3^{-}S2^{+}CD19^{+}$) in
181 mesenteric lymph nodes were significantly higher than those in spleen
182 (Supplementary Figure 3B). To further clarify the role of fecal microbiota in the
183 induction of S2 cross-reactive antibodies, mice from isolation pack were
184 transplanted with fecal bacteria prepared from SPF mice (Figure 4C). We
185 found that P144 specific antibodies significantly increased after fecal
186 microbiota transplantation (FMT) (Figure 4D). These results collectively
187 suggested that the S2 cross-reactive antibodies might be induced by
188 exposures to certain microbial antigens.
189
190 **P144 specific monoclonal antibodies reacted with commensal gut**
191 **bacteria from both human and mouse and showed limited neutralizing**
192 **activities**
193 To probe the potential antigens that might induce the P144 binding antibodies,
194 we isolated 6 mAbs from two naïve SPF mice (one C57BL/6J mouse and one
195 BALB/c mouse) with high levels of pre-existing S2 specific antibody responses.
196 Five of these mAbs recognized P144 solely, while one mAb (clone M3) bound
197 with P144 and P103 simultaneously (Supplementary Figure 4B). Results of
198 competitive ELISA showed that the minimal epitopes varied slightly among the
199 five P144 specific mAbs, especially at the C-terminal of P144 (Supplementary
200 Figure 4A). The neutralizing potentials of these isolated monoclonal antibodies
201 were evaluated using a pseudo virus-based neutralization assay. Our results
202 showed that these monoclonal antibodies exhibited limited neutralizing activity
203 against 5 major SARS-CoV-2 variants (Supplementary Figure 5). Of note, G18
204 neutralized the Indian strain (B.1.617) by 31%; F5 neutralized the UK strain
205 (B.1.1.7) and the South African strain (B.1.351) by around 20%; G13

206 neutralized the South African strain (B.1.351) by nearly 20% (Supplementary
207 Figure 5).
208 To prove the cross-reactivities between S2 and commensal gut microbial
209 antigens, whole cell lysates (WCL) of mouse and human commensal gut
210 bacteria were prepared and used as antigens for Western blotting assays,
211 respectively. As shown in Figure 5A, specific bindings with the WCL of mixed
212 fecal bacteria prepared from mice either with low levels of pre-existing
213 antibodies (L) or with high levels of pre-existing antibodies (H) could be clearly
214 visualized for each isolated mAbs. It was noteworthy that all mAbs except E10
215 strongly recognized a band around 180KD in the sample from mice with high
216 pre-existing antibody responses. E10 predominantly recognized a band
217 around 55KD in both samples, while stronger binding with the sample from
218 mice with high pre-existing antibody responses could be visually observed
219 (Figure 5A). Among the six mAbs, F5 showed the most diverse binding
220 compacity. In addition to the band around 180KD, F5 bound with a band
221 around 55KD (similar with E10) and a band between 40KD-55KD (Figure 5A).
222 In comparison with the WB results of mouse samples, the recognized bands
223 were less consistent across different human fecal bacteria samples (Figure
224 5B), presumably due to the individual to individual variation of gut microbiota
225 composition. We found that a band around 70KD was recognized by most
226 mAbs in 4 (lanes 1, 5, 6, 7) out of 7 samples and a band between 50KD-70KD
227 was recognized by all mAbs in 3 (Lanes 2, 3, 7) out 7 samples. Besides, our
228 data showed that the recognition pattern of each sample was largely
229 consistent across different mAbs (Figure 5B).
230 Proteins corresponding to specifically recognized bands were excised from
231 Coomassie blue stained gels and analyzed by the mass spectrometry. For the
232 mouse fecal bacteria samples, protein bands with molecular weights around
233 180KD, 100KD, 55KD-70KD and 40KD-55KD (indicated by arrows in Figure
234 5A, panel F5) were selected. For human fecal bacteria samples, protein bands
235 with molecular weights around 50KD-70KD, 70KD and 70KD-100KD
236 (indicated by arrows in Figure 5B, panel F5) were selected. The lists of
237 proteins identified in mouse and human samples were shown in Table 2 and
238 Table 3, respectively. Proteins with molecular weights corresponding
239 approximately to the excised protein bands were identified for both human and
240 mouse fecal bacteria samples. Of note, multiple proteins within the theoretical

241 MW range of 58KD to 60KD were found to be identical between mouse and
242 human samples, which included Fumarate hydratase class I (Accession#
243 P14407), Formate-tetrahydrofolate ligase OS (Accession# Q189R2),
244 Phosphoenolpyruvate carboxykinase (ATP) OS (Accession# C4ZBL1 and
245 A6LFQ4) and 60 kDa chaperonin OS (Accession# A0Q2T1). To verify the
246 cross-reactivity of the proteins detected by LC-MS, we selected E. coli (DH5α
247 strain) as a representative target because *E. coli* derived Fumarate hydratase
248 class I (Accession# P14407) were found in both human and mouse fecal
249 bacteria samples. The result of WB assay showed that the P144 specific mAb
250 (clone F5) recognized multiple bands with MWs consistent with *E. coli* proteins
251 identified by LC-MS (Supplementary Figure 6).
252

253 **Pre-existing S2 cross-reactive antibodies impacted specific immunities**
254 **induced by a candidate COVID-19 DNA vaccine in mice**

255 Pre-existing antibodies has been shown to be able to shape the recall immune
256 responses upon influenza infection and vaccination (6). And the concern about
257 how the pre-existing immunities may influence the effect of a SARS-CoV-2
258 vaccine has also attracted lots of attention (33). To investigate the impact of
259 the pre-existing P144 antibodies on the immunogenicity of a candidate DNA
260 vaccine, 18 BALB/c mice were divided into 3 groups according to their levels of
261 pre-existing S2 binding antibodies and immunized with a DNA vaccine
262 encoding the full length of SARS-CoV-2 S protein (Figure 6A and 6B). Our data
263 showed that mice with high levels of pre-existing S2 binding antibodies
264 mounted significantly higher S2 binding antibody responses after vaccination
265 compared to mice with low or moderate levels of pre-existing S2 binding
266 antibodies (Figure 6C). More specifically, the average level of P144 specific
267 antibody responses was also stronger in mice with high levels of pre-existing
268 S2 binding antibodies than mice with low levels of pre-existing S2 binding
269 antibodies (Figure 6D and 6E). By comparison, both the S1 binding antibody
270 and the neutralizing antibody titers did not significantly differ among all groups,
271 despite that mice with moderate or high levels of pre-existing antibodies
272 tended to mount higher average titer of S1 binding antibodies (Figure 6F and
273 6G). Mice without vaccination showed neither obvious S1 binding antibody
274 response nor neutralizing activity (Data not shown). We further investigated
275 the influence of pre-existing antibodies on humoral immune responses in

276 mouse respiratory tract after vaccination. And our data showed that the levels
277 of S1 specific IgG in BALF were similar among the three groups after DNA
278 vaccination (Figure 7A), while the average level of S2 specific IgG in BALF
279 from mice with high pre-existing S2 binding antibodies was significantly higher
280 than those from mice with low pre-existing antibodies (Figure 7B). S protein
281 specific IgA response did not increase significantly after vaccination as
282 compared with unvaccinated group (Figure 7C and 7D).
283 As most pre-existing antibodies in naïve SPF mice recognized P144 (Figure
284 2C and Supplementary Figure 1), we delineated the impact of pre-existing
285 antibody on the epitope recognition after vaccination. Our results showed that
286 the minimum epitope recognition pattern by the sera of mice with high levels of
287 pre-existing antibodies remained unchanged after vaccination (Figure 8).
288 Whereas the minimum epitope recognized by the sera of mice with moderate
289 and low levels of pre-existing antibody responses altered at either the
290 N-terminal or both terminals of P144 (Figure 8).
291 In addition to antibody measurement, we compared S protein specific T cell
292 responses among the three groups as well (Figure 9A). The results showed
293 that the candidate DNA vaccine elicited robust S protein specific T cell
294 responses in all groups (Figure 9). Although no statistical significance was
295 reached, interesting trends were observed: First, mice with high levels of
296 pre-existing S2 binding antibodies tended to mount relatively higher S1
297 specific cellular immune responses (Figure 9B, 9C and 9D); second, as
298 measured by the total responses of IL-6, IL-2 and TNF-a, mice with high levels
299 of pre-existing antibodies tended to mount stronger T cell responses against
300 S1 while lower responses against S2 (Figure 9C and 9D). Mice without
301 vaccination showed no S protein specific T cells responses (Data not shown).
302
303 **Pre-existing S2 cross-reactive antibodies correlated with RBD binding**
304 **antibody responses after two-dose inactivated SARS-CoV-2 vaccination**
305 To investigate how the pre-existing cross-reactive antibodies may influence the
306 COVID-19 vaccine induced immunity, peripheral blood samples were collected
307 from 28 healthy individuals who received two doses of an inactivated
308 SARS-CoV-2 vaccine (Fig.10A). Correlation analyses showed that the levels
309 of pre-existing P144 and S2 binding antibodies were significantly associated
310 with RBD binding antibody titers at 14 days after immunization (Fig.10 B and

311 10E). Additionally, although not statistically significant, the pre-existing P144
312 binding antibody levels tended to correlate positively with neutralizing antibody
313 responses after vaccination (P=0.0946) (Fig.10D).
314
315 **Discussion**
316 The origins of pre-existing cross-reactive immunities against SARS-CoV-2
317 have been investigated vigorously since the outbreak of the pandemic (39).
318 Accumulating data suggest that cross-reactive T cells (33, 40-43) in
319 SARS-CoV-2 unexposed human might be induced by previous infections of
320 other hCoVs. While the origins of pre-existing cross-reactive antibodies could
321 not be completely explained by previous infections of other coronaviruses, as
322 recent studies revealed that the magnitude of antibody responses to
323 SARS-CoV-2 S protein in the sera of patients with COVID-19 was not related
324 to HCoVs' S titers (44) and immunization with coronaviruses OC43 did not
325 induce significant SARS-CoV-2 S protein cross-reactive antibodies in mice.
326 Moreover, it has also been observed that SARS-CoV-2 S protein specific
327 binding antibody responses were weak in SARS-CoV-2 unexposed individuals
328 with obvious binding antibody responses against S proteins of common cold
329 hCoVs (45, 46).
330 To track the potential origins of the pre-existed cross-reactive antibodies
331 targeting SARS-CoV-2 spike protein, in this study, we first screened the
332 cross-reactive antibody responses in SARS-CoV-2 unexposed human plasma
333 collected in 2020 and 2016, respectively. In both cohorts, we found that the
334 magnitudes of S2 binding antibodies were significantly higher than those of S1
335 binding antibodies. This finding is consistent with previous studies showing
336 that pre-existing S2 cross-reactive antibody responses are stronger than S1
337 cross-reactive antibody responses in SARS-CoV-2 unexposed individuals (44,
338 47, 48). Since S2 cross-reactive antibody responses have also been observed
339 in unexposed animals (44), we continued to screen the cross-reactive antibody
340 responses in two strains of naïve SPF mice. Our data showed that the OD
341 values of S2 cross-reactive antibodies were significantly higher than those of
342 S1 cross-reactive antibodies in naïve BALB/c and C57BL/6 mice. Detections of
343 mouse sera collected from another two independent SPF animal facilities
344 confirmed this finding (Data not shown). We also tried to detect the
345 SARS-CoV-2 S protein specific T cells responses in mice with high

346 pre-existing S2 cross-reactive antibodies using the IFN-γ ELISPOT assay,
347 which showed that there was no pre-existing cross-reactive T cell response.
348 To facilitate the search of potential antigens that induced the cross-reactive
349 antibodies, we identified a dominant antibody epitope (P144) through a
350 method of competitive ELISA based linear antibody epitope mapping. P144 is
351 located within the connector domain of S2 (aa1147-aa1160, directly N-terminal
352 of the HR2 region). The same epitope has been predicted (38) and detected in
353 both SARS-CoV-2 unexposed and infected individuals by multiple previous
354 studies (22, 23, 25, 26, 32). In this study, we also detected P144 specific
355 antibody responses in plasma of healthy individuals collected in both 2020 and
356 2016. More interestingly, we found that the pre-existing S2 cross-reactive
357 antibodies in mice were predominantly against the single epitope. Of note,
358 although the aa sequence of P144 is highly conserved between SARS-CoV-2
359 and SARS-CoV, its similarity with four seasonal hCoVs is relatively low. A
360 recent study showed that this epitope was more frequently recognized than its
361 homologous peptides from common cold hCoVs by antibodies in plasma of
362 COVID-19 negative individuals (23). The above evidence implied again that
363 the pre-existing S2 specific antibodies might not be necessarily elicited by
364 previous common cold coronavirus infections.
365 As the pre-existing S2 binding antibodies in mice were predominantly against
366 P144, it provided us a good chance to unveil their origins. To do so, we first
367 labeled mouse B cells with purified S2 protein and found that the frequency of
368 S2 specific B cells was significantly higher in mesenteric LN than in spleen,
369 suggesting that the gastrointestinal tract might be the primary site where the
370 cross-reactive B cells were activated. Exposure to a certain gut microbial
371 antigen, which can promote B cell diversification and stimulate antibody
372 production in both T-dependent and -independent ways (49), might account for
373 the presence of the cross-reactive antibodies. To prove this hypothesis, we
374 next compared the levels of pre-existing S2 cross-reactive antibodies between
375 mice housed in a sterile isolation pack and mice maintained in SPF condition.
376 Our results showed that the levels of pre-existing S2 cross-reactive antibodies
377 were significantly higher in SPF mice. Through metagenomic sequencing, we
378 further demonstrated that the abundance of bacteroidaceae, prevotellaceace
379 and parabacteroides were also significantly higher in the commensal gut
380 bacteria of SPF mice. Moreover, we found that transplantation of fecal

381 microbiota from SPF mice could induce P144 cross reactive antibodies in mice
382 bred in the isolation pack. These evidences suggested that the S2
383 cross-reactive antibodies could be induced by certain commensal gut bacteria.
384 To identify the potential cross-reactive bacterial antigens, we isolated six P144
385 specific monoclonal antibodies from a naïve BALB/c mouse and a naïve
386 C57BL/6 mouse, respectively. All the six mAbs were confirmed to be able to
387 bind with P144 and showed weak neutralizing compacities against five
388 SARS-CoV-2 variants. Leveraging these mAbs, we detected the
389 cross-reactive antigens in mouse and human fecal microbiota through WB
390 assays. Compared with a control mouse IgG, specific bands were observed for
391 each mAb, which proved the antibody cross-reactivities between SARS-CoV-2
392 and commensal gut bacteria. The strongly recognized protein bands were
393 further analyzed by LC-MS. Our data showed that cross-reactive antigens
394 derived from bacteroides and parabacteroides were frequently identified in
395 fecal bacteria samples of both human and mouse, which was consistent with
396 our metagenomic sequencing data showing that the abundance of bacteroides
397 and parabacteroides was significantly higher in the commensal gut bacteria of
398 mice with high pre-existing S2 binding antibody levels. More intriguingly, five
399 cross-reactive microbial antigens were identified in mouse and human fecal
400 samples simultaneously, which implied that the S2 cross-reactive antibodies
401 might naturally occur in different species of mammals. We also analyzed the
402 sequence similarities between P144 and the proteins identified by LC-MS. Our
403 results showed that most identified proteins shared varied identities with P144
404 (40%-70%, for more than 8 residues) (Data not shown). The cross-reactive
405 epitopes on the identified proteins could not be specified based on our current
406 data. Besides, the neutralizing mechanism(s) of P144 specific antibodies and
407 their potential influences on gut microbiota were not clarified in this study. We
408 plan to look into these issues in future.
409 In parallel with tracking the initial antigens that induced the S2 cross-reactive
410 antibodies, we investigated the impact of pre-existing antibodies on the
411 immunogenicity of a candidate DNA vaccine as well. According to previous
412 reports, pre-existing cross-reactive antibodies may influence the effects of
413 different vaccines differentially (6, 50). In this study, we found that the
414 pre-existing cross-reactive antibodies shaped the vaccine-induced immune
415 responses in both mouse and human. Mice with high levels of pre-existing

416 antibodies mounted stronger S2 binding antibodies in both peripheral blood
417 and bronchial lavage after vaccination. More interestingly, we found that the
418 pre-existing antibody levels correlated positively with post-vaccination RBD
419 binding antibody titers in human. These findings proved that the pre-existing
420 S2 binding antibodies could facilitate the generation of vaccine induced
421 antibody responses. Through epitope mapping, we observed that the
422 pre-existing antibodies strongly restricted the minimal epitope recognition in
423 mice with high levels of pre-existing antibodies, which suggested that the
424 imprint effect of pre-existing cross-reactive antibodies on vaccine induced
425 antibody responses was primarily epitope specific. In addition to antibody
426 response, we also found that the high levels of pre-existed S2 binding
427 antibodies tended to induce higher S1 specific T cell responses while lower S2
428 specific T cell responses, implying that the pre-existing antibodies might
429 change the balance between humoral versus cellular immune responses
430 against the cross-reactive antigen. Since we did not perform the live virus
431 challenge, it is still not clear how the pre-existing cross-reactive antibodies will
432 impact vaccine efficacy *in vivo*. Nonetheless, as both our results and a recently
433 published study suggested that antibodies targeting P144 epitope could
434 neutralize SARS-CoV-2(51), we speculate that the pre-existing P144
435 cross-reactive antibodies may have protective effect.
436 A deep understanding of pre-existing cross-reactive antibodies against
437 SARS-CoV-2 will enable better therapeutic, diagnostic and vaccine strategies.
438 In this study, we provided evidence showing that antibodies targeting a
439 conserved linear epitope on S2 cross-reacted with gut microbial antigens from
440 both human and mouse, manifesting that some of the pre-existing
441 cross-reactive antibodies might be induced by exposure to certain commensal
442 gut bacteria. We proved that the pre-existing S2 cross-reactive antibodies did
443 not impair the immunogenicity of a candidate DNA vaccine in a mouse model.
444 Further investigations into the role of P144 specific antibody after
445 SARS-CoV-2 infection and its impact on gut microbiota might provide clues to
446 elucidate the mechanisms underlying the gastrointestinal symptom of
447 COVID-19 (52-54).
448
449 **Materials and methods**
450 **Ethics statement**

451 All experiments and methods were performed in accordance with relevant
452 guidelines and regulations. Experiments using mice and samples of healthy
453 human were approved by the Research Ethics Review Committee of the
454 Shanghai Public Health Clinical Center Affiliated to Fudan University. The
455 study involving 28 healthy vaccinees was reviewed and approved by the
456 institutional ethics committee of Hubei provincial CDC, China.
457
458 **Plasma samples of healthy human**
459 Two batches of plasma samples were collected from healthy individuals at the
460 health screening clinic of Shanghai Public Health Clinical Center. A concurrent
461 batch was collected in December 2020. All the 95 individuals enrolled in this
462 batch reported no epidemiological link with confirmed COVID-19 patients and
463 were confirmed to be free from any chronic or acute disease. Viral RNA tests
464 confirmed that all individuals in this batch were free from SARS-CoV-2
465 infection. In addition, a historical batch of 78 plasma samples from healthy
466 individual cohort (collected in 2016) were also measured for their cross
467 reactivities with SARS-CoV-2 S protein. Demographical information about
468 these two cohorts was described in Table 1.
469
470 **Detection of SARS-CoV-2 S1 and S2 specific binding antibodies**
471 In-house enzyme-linked immunosorbent assays (ELISA) were developed to
472 measure SARS-CoV-2 S1 and S2 specific binding antibodies. High-binding
473 96-well EIA plates (Cat# 9018, Corning, USA) were coated with purified
474 SARS-CoV-2 S1 (Cat# 40591-V08H, Sino Biological, China) or S2 proteins
475 (Cat# 40590-V08B, Sino Biological, China) at a final concentration of 1μg/ml in
476 carbonate/bi-carbonate coating buffer (30mM $NaHCO_3$,10mM Na_2CO_3, pH
477 9.6). Subsequently, the plates were blocked with 1×PBS containing 5% milk
478 for 1 hour at 37°C. Next, 100μl of diluted human plasma or mouse serum was
479 added to each well. After 1-hour incubation at 37°C, the plates were washed
480 with 1×PBS containing 0.05% Tween20 for 5 times. Then, 100μl of a HRP
481 labeled goat anti-mouse IgG antibody (Cat# ab6759, Abcam, UK) or goat
482 anti-mouse IgG antibody (Cat# 115-035-003, Jackson Immuno Research, USA)
483 diluted in 1×PBS containing 5% milk were added to each well and incubated
484 for 1 hour at 37°C. After a second round of wash, 100μl of TMB substrate
485 reagent (Cat# MG882, MESGEN, China) was added to each well. 15 minutes

486 later, the color development was stopped by adding 100μl of 1M H_2SO_4 to
487 each well and the values of optical density at $OD450_{nm}$ and $OD630_{nm}$ were
488 measured using 800 TS microplate reader (Cat# 800TS, Biotek, USA).
489
490 **Competitive ELISA**
491 According to the reference sequence of SARS-CoV-2 (Genebank accession
492 number: NC_045512), peptides (18-mer overlapping by 11 residues, purities >
493 95%) encompass the full length of S protein were synthesized by GL Biochem
494 (Shanghai, China). The experiment procedure was generally similar with the
495 afore mentioned in-house ELISA assays, except that the diluted mouse serum
496 or human plasma were incubated with synthesized peptides (5μg/ml) for 1
497 hour at room temperature before adding into the coated EIA plates. 1×PBS
498 containing 0.01% DMSO (the solvent used to dissolve peptides) were used as
499 the negative control in this assay.
500
501 **Antibody avidity assay**
502 Avidity of Ag-specific Ab was determined by ELISA as reported (55) with minor
503 modifications. Briefly, plates were coated as the regular ELISA assay
504 described above. Diluted (1:200) mouse sera were added into each well. After
505 1-hour incubation, ELISA plates were washed with washing buffer and
506 incubated with 1.5M NaSCN or PBS for 15 mins at room temperature and then
507 immediately washed with washing buffer. Ab avidity index was defined as the
508 ratio of the OD value of a sample with 1.5M NaSCN treatment versus the OD
509 value of the same sample with PBS treatment.
510
511 **FACS analysis of S2 specific B cells in mice**
512 Spleen and mesenteric lymph nodes were isolated from naïve SPF mice and
513 single-cell suspensions were freshly prepared. After counting, 1×10^6 single
514 cells were resuspended in 100μl R10 (RPMI1640 containing 10% fatal bovine
515 serum) and incubated with biotinylated S2 protein (Cat# 40590-V08B-B, Sino
516 Biological, China) for 30 minutes at room temperature. After incubation, the
517 cells were washed twice with 500μl R10. Then, the cells were incubated with
518 the mixture of PE-anti-mouse CD19 (Cat# 152408, Biolegend, USA, 1μl/test),
519 BV510-anti-mouse CD45 (Cat# 103137, Biolegend, USA, 1.25μl/test) and
520 Streptavidin-IF647 (Cat# 46006, AAT Bioquest, USA, 0.2μl/test) at room

521 temperature for 30 minutes. After washing, the stained cells were resuspended
522 in 200μl 1×PBS and analyzed using a BD LSRFortessa™ Flow Cytometer.
523 The data were analyzed using the FlowJo software (BD Biosciences, USA).
524
525 **Preparation of P144 specific monoclonal antibodies**
526 Monoclonal antibodies against P144 were prepared from one naïve BALB/c
527 mouse and one naïve C57BL/6 mouse respectively using the hybridoma
528 technique. Briefly, freshly isolated splenocytes were mixed and fused with
529 SP2/0 cells at a ratio of 1:10. Hybridoma cell clones secreting P144 specific
530 antibodies were screened by ELISA and monoclonal hybridoma cells were
531 selected by multiple rounds of limited dilution. Selected clones of hybridoma
532 cells were injected intraperitoneally into BALB/c×ICR hybrid mice. About 1-2
533 weeks later, peritoneal fluid was collected, and monoclonal IgG was purified
534 using Protein A resin. The purities of monoclonal antibodies were verified using
535 SDS-PAGE and the antibody concentrations were determined using a BCA kit
536 (Cat# P0012, Beyotime Biotechnology, China).
537
538 **Isolation of gut commensal bacteria and preparation of whole cell lysate**
539 **(WCL)**
540 About 2g of each fecal sample was suspended with 15ml sterile 1×PBS and
541 vortexed thoroughly to obtain uniform mixtures. After centrifugation at 200×g
542 for 5 min, the supernatants were collected, and the sediments were discarded.
543 This process was repeated twice. Next, all the supernatant samples were
544 centrifuged twice at 9000×g for 5 min and the supernatants were discarded.
545 The precipitated bacteria pellets were resuspended in 500μl of 1×PBS
546 (containing 1mM PMSF) and disrupted with an ultrasonic cell crusher (the
547 probe-type sonicator, Model JY92-II; Ningbo Scientz Biotechnology Co., Ltd,
548 China). After sonication, the samples were centrifuged at 10000rpm for 30
549 minutes to remove the cellular debris.
550
551 **Western blotting**
552 WCL containing 10μg of total protein was separated by SDS-PAGE (10%
553 acrylamide gels) and then transferred onto a PVDF membrane (Cat#
554 IPVH00010, Millipore, USA) or stained with Coomassie brilliant blue. After
555 blocking with 5% skim milk for 2h, the membrane was incubated with a P144

556 specific monoclonal antibody or a control mouse IgG at a concentration of 1
557 μg/ml. After washing, the membrane was incubated with HRP conjugated goat
558 anti-mouse IgG antibody (Cat # ab6759, Abcam, UK) diluted 1:5000 in TBST
559 (Tris-buffered saline, pH 8.0, 0.05% Tween 20) containing 5% skim milk. After
560 wash, the bands were developed with an ultra-sensitive ECL substrate (Cat#
561 K-12045-D10, Advansta, USA). The area corresponding to the specific WB
562 bands were excised from the gel stained with Coomassie blue and analyzed
563 using the mass spectrometry.
564
565 **Mass spectrometry analysis**
566 The FASP digestion was adapted for the following procedures in Microcon
567 PL-10 filters. After three-time buffer displacement with 8 M Urea and 100 mM
568 Tris-HCl, pH 8.5, proteins were reduced by 10 mM DTT at 37 °C for 30 min and
569 followed by alkylation with 30 mM iodoacetamide at 25°C for 45 min in dark.
570 Digestion was carried out with trypsin (enzyme/protein as 1:50) at 37°C for 12
571 h after a wash with 20% ACN and three-time buffer displacement with
572 digestion buffer (30 mM Tris-HCl, pH 8.0). After digestion, the solution was
573 filtrated out and the filter was washed twice with 15% ACN, and all filtrates
574 were pooled and vacuum-dried to reach a final concentration to 1 mg/ml.
575 LC-MS analysis was performed using a nanoflow EASYnLC 1200 system
576 (Thermo Fisher Scientific, Odense, Denmark) coupled to an Orbitrap Fusion
577 Lumos mass spectrometer (Thermo Fisher Scientific, Bremen, Germany). A
578 one-column system was adopted for all analyses. Samples were analyzed on
579 a home-made C18 analytical column (75 μm i.d. × 25 cm, ReproSil-Pur 120
580 C18-AQ, 1.9 μm (Dr. Maisch GmbH, Germany)). The mobile phases consisted
581 of Solution A (0.1% formic acid) and Solution B (0.1% formic acid in 80% ACN).
582 The derivatized peptides were eluted using the following gradients: 2–5% B in
583 2 min, 5–35% B in 100 min, 35–44% B in 6 min, 44–100% B in 3 min, 100% B
584 for 10 min, at a flow rate of 200 nl/min. Data-dependent analysis was
585 employed in MS analysis: The time between master scan was 3s, and
586 fragmented in HCD mode, normalized collision energy was 30.
587
588 **Construction and preparation of a candidate DNA vaccine encoding**
589 **SARS-CoV-2 full length S protein**
590 The full-length *s* gene sequence of the reference SARS-CoV-2 strain was

591 optimized according to the preference of human codon usage and synthesized
592 by GENEWIZ life science company (Suchow, China). The codon optimized
593 spike gene was subcloned into a eukaryotic expression vector (pJW4303,
594 kindly gifted by Dr. Shan Lu's Laboratory at the University of Massachusetts)
595 (56). And the sequence of inserted gene was verified by Sanger sequencing
596 (Sangon Biotech Co., Ltd., Shanghai, China). An EndoFree Plasmid
597 Purification Kit (Cat#12391, Qiagen, Hilden, USA) was used to prepare the
598 recombinant plasmid for mouse vaccination.
599
600 **Mouse vaccination**
601 Peripheral blood samples were collected from female adult mice and
602 pre-existing S2 binding antibodies were measured using the previously
603 described in-house ELISA method. According to their pre-existing S2 binding
604 antibody levels (at 1:100 dilution of serum), the mice were divided into three
605 groups: low ($0.015 < OD_{450nm-630nm} \leqslant 0.130$, n=6), moderate ($0.130 <$
606 $OD_{450nm-630nm} \leqslant 0.750$, n=6) and high ($OD_{450nm-630nm} > 0.750$, n=6). All mice
607 were immunized intramuscularly with the candidate S protein DNA vaccine
608 (50μg/mouse) for three times at an interval of 2 weeks. Three weeks post the
609 third vaccination, the mice were euthanized. Peripheral blood, bronchial lavage
610 and spleen were collected for assays of S protein specific immune responses.
611
612 **Metagenomic analysis of mouse gut microbiota**
613 Stool (fecal) samples were self-collected and DNA was extracted from 250 mg
614 of each fecal sample in duplicate. The DNA samples were separated strictly
615 according to TIANamp Stool DNA Kit (Cat# DP328, TIANGEN, China). Then, a
616 total amount of 1μg DNA per sample was used as input material for the DNA
617 sample preparations. Sequencing libraries were generated using NEBNext®
618 Ultra™ DNA Library Prep Kit for Illumina (NEB, USA) following manufacturer's
619 recommendations and index codes were added to attribute sequences to each
620 sample. Briefly, the DNA sample was fragmented by sonication to a size of
621 350bp, then DNA fragments were end-polished, A-tailed, and ligated with the
622 full-length adaptor for Illumina sequencing with further PCR amplification. At
623 last, PCR products were purified (AMPure XP system) and libraries were
624 analyzed for size distribution by Agilent 2100 Bioanalyzer and quantified using
625 real-time PCR. The clustering of the index-coded samples was performed on a

626 cBot Cluster Generation System according to the manufacturer's instructions.
627 After cluster generation, the library preparations were sequenced on an
628 Illumina Novaseq 6000 platform and paired-end reads were generated.
629
630 **SARS-CoV-2 pseudo-virus neutralization assay**
631 VSV-backboned SARS-CoV-2 pseudo-viruses were prepared according to a
632 reported method (57). The neutralization assay was conducted by following
633 the previously described procedure (57, 58). Briefly, 100μl of serially diluted
634 mice sera were added into 96-well cell culture plates. Then, 50μl of
635 pseudo-viruses with a titer of 13000 $TCID_{50}$/ml were added into each well and
636 the plates were incubated at 37°C for 1 hour. Next, Vero cells were added into
637 each well (2×10^4 cells/well) and the plates were incubated at 37°C in a
638 humidified incubator with 5% CO_2. 24 hours later, luminescence detection
639 reagent (Bright-Glo™ Luciferase Assay System, Promega, USA) was added to
640 each well following the manufacturer`s instruction. The luminescence was
641 measured using a luminescence microplate reader (GloMax®
642 Navigator Microplate Luminometer, Promega, USA) within 5 minutes. The
643 Reed-Muench method was used to calculate the virus neutralization titer.
644 Antibody neutralization titers were presented as 50% maximal inhibitory
645 concentration (IC_{50}).
646
647 **Detections of S protein specific cellular immune responses**
648 SARS-CoV-2 S protein specific IFN-γ releases were measured using the
649 method of enzyme-linked immunosorbent spot (ELISPOT) assays (Cat#
650 551083, BD Bioscience, USA) according to a previously described procedure
651 (59). Briefly, the 96-well ELISPOT plates were coated with purified anti-mouse
652 IFN-γ monoclonal antibody overnight at 4°C. Then, the plates were blocked
653 and 2×10^5 fresh splenocytes were added into each well and incubated with
654 peptide pools for 20 hours at 37°C in a humidified incubator with 5% CO_2. The
655 final concentration for each peptide was 1μg/ml. After incubation, detecting
656 antibody and Avidin-HRP were added sequentially. Finally, the plates were
657 developed using the BD™ ELISPOT AEC Substrate Set (Cat#551951, BD
658 Bioscience, USA) according to the manufacturer's manual. Spots representing
659 IFN-γ producing cells were enumerated using an automated ELISPOT plate
660 reader (ChampSpot III Elispot Reader, Saizhi, Beijing, China). At the same

661 time, the supernatants in the wells of ELISPOT plates were also collected for
662 detecting secreted cytokines using a multiplexed cytokine beads array kit
663 (Cat# 741054, Biolegend, USA).
664
665 **Statistical analysis**
666 All statistical analyses were performed using GraphPad Prism 8
667 (GraphPad Software, Inc., La Jolla, CA, USA). Comparisons between two
668 groups were conducted by the method of *t*-test. Comparisons among three or
669 more group were done using one-way ANOVA. $P<0.05$ was considered as
670 statistically significant.
671
672 **Acknowledgements**
673 We thank Miss Zhangyufan He from Huashan Hospital, Fudan University, for
674 her kind help with the language polishing. This work was funded by the
675 National Natural Science Foundation of China (Grant No. 81971559,
676 82041010, 81971900, 31872744), National Science and Technology Major
677 Project (Grant No. 2018ZX10731301-004, 2018ZX10302302-002 and
678 2018ZX10301-404-002-003) and the Science and Technology Commission of
679 Shanghai Municipality (Grant No. 20411950400).
680
681 **Author contributions**
682 Y.M.W., Y.X., C.Q., Z.Q.Z. and W.H.Z. designed the study. L.Q.J., S.F.W.,
683 Y.M.W., X.X.T., Y.F.Z., J.W., X.Y.W., and J.W. conducted the experiments.
684 Y.M.W., L.Q.J. and S.F.W. analyzed the data and drafted the manuscript.
685 Y.M.W., Y.X., C.Q., Z.Q.Z. and W.H.Z. revised the manuscript. D.M.Y. and
686 W.H.W. provided intellectual inputs in tackling technical challenges in tracking
687 the potential cross-reacting antigens.
688
689 **Conflict of Interest**
690 The authors declare that they have no relevant conflicts of interest.
691
692 **Data availability**
693 The data of metagenomic analysis of gut microbiota has been deposited to the

694 NCBI Sequence Read Archive (SRA) database with the accession number
695 PRJNA747837.
696

697 **References**

698 1. Lu LL, Suscovich TJ, Fortune SM, Alter G. Beyond binding: antibody effector functions in
699 infectious diseases. Nature reviews Immunology. 2018;18(1):46-61.
700 2. Warter L, Appanna R, Fink K. Human poly- and cross-reactive anti-viral antibodies and their
701 impact on protection and pathology. Immunologic research. 2012;53(1-3):148-61.
702 3. Cobey S, Hensley SE. Immune history and influenza virus susceptibility. Current opinion in
703 virology. 2017;22:105-11.
704 4. Mok DZL, Chan KR. The Effects of Pre-Existing Antibodies on Live-Attenuated Viral Vaccines.
705 Viruses. 2020;12(5).
706 5. Zimmermann P, Curtis N. Factors That Influence the Immune Response to Vaccination. Clinical
707 microbiology reviews. 2019;32(2).
708 6. Dugan HL, Guthmiller JJ, Arevalo P, Huang M, Chen YQ, Neu KE, et al. Preexisting immunity
709 shapes distinct antibody landscapes after influenza virus infection and vaccination in humans. Science
710 translational medicine. 2020;12(573).
711 7. Zhang A, Stacey HD, Mullarkey CE, Miller MS. Original Antigenic Sin: How First Exposure
712 Shapes Lifelong Anti-Influenza Virus Immune Responses. Journal of immunology (Baltimore, Md :
713 1950). 2019;202(2):335-40.
714 8. Boes M. Role of natural and immune IgM antibodies in immune responses. Molecular
715 immunology. 2000;37(18):1141-9.
716 9. Auladell M, Jia X, Hensen L, Chua B, Fox A, Nguyen THO, et al. Recalling the Future:
717 Immunological Memory Toward Unpredictable Influenza Viruses. Frontiers in immunology.
718 2019;10:1400.
719 10. St. John AL, Rathore APS. Adaptive immune responses to primary and secondary dengue virus
720 infections. Nature Reviews Immunology. 2019;19(4):218-30.
721 11. Izmirly AM, Alturki SO, Alturki SO, Connors J, Haddad EK. Challenges in Dengue Vaccines
722 Development: Pre-existing Infections and Cross-Reactivity. 2020;11(1055).
723 12. Andrade P, Gimblet-Ochieng C, Modirian F, Collins M, Cárdenas M, Katzelnick LC, et al. Impact
724 of pre-existing dengue immunity on human antibody and memory B cell responses to Zika. Nature
725 Communications. 2019;10(1):938.
726 13. Liao HX, Chen X, Munshaw S, Zhang R, Marshall DJ, Vandergrift N, et al. Initial antibodies
727 binding to HIV-1 gp41 in acutely infected subjects are polyreactive and highly mutated. The Journal of
728 experimental medicine. 2011;208(11):2237-49.
729 14. Bonsignori M, Liao HX, Gao F, Williams WB, Alam SM, Montefiori DC, et al. Antibody-virus
730 co-evolution in HIV infection: paths for HIV vaccine development. Immunological reviews.
731 2017;275(1):145-60.
732 15. Williams WB, Liao HX, Moody MA, Kepler TB, Alam SM, Gao F, et al. HIV-1 VACCINES.
733 Diversion of HIV-1 vaccine-induced immunity by gp41-microbiota cross-reactive antibodies. Science
734 (New York, NY). 2015;349(6249):aab1253.
735 16. Zitvogel L, Ayyoub M, Routy B, Kroemer G. Microbiome and Anticancer Immunosurveillance.
736 Cell. 2016;165(2):276-87.

17. Leng Q, Tarbe M, Long Q, Wang F. Pre-existing heterologous T-cell immunity and neoantigen immunogenicity. Clinical & translational immunology. 2020;9(3):e01111.
18. Sioud M. T-cell cross-reactivity may explain the large variation in how cancer patients respond to checkpoint inhibitors. Scandinavian journal of immunology. 2018;87(3).
19. Rose NR. Negative selection, epitope mimicry and autoimmunity. Current opinion in immunology. 2017;49:51-5.
20. Anderson EM, Goodwin EC, Verma A, Arevalo CP, Bolton MJ, Weirick ME, et al. Seasonal human coronavirus antibodies are boosted upon SARS-CoV-2 infection but not associated with protection. Cell. 2021.
21. Galipeau Y, Greig M, Liu G, Driedger M, Langlois MA. Humoral Responses and Serological Assays in SARS-CoV-2 Infections. Frontiers in immunology. 2020;11:610688.
22. Klompus S, Leviatan S, Vogl T, Kalka IN, Godneva A, Shinar E, et al. Cross-reactive antibody responses against SARS-CoV-2 and seasonal common cold coronaviruses. 2020:2020.09.01.20182220.
23. Shrock E, Fujimura E, Kula T, Timms RT, Lee IH, Leng Y, et al. Viral epitope profiling of COVID-19 patients reveals cross-reactivity and correlates of severity. Science (New York, NY). 2020;370(6520).
24. Ortega N, Ribes M, Vidal M, Rubio R, Aguilar R, Williams S, et al. Seven-month kinetics of SARS-CoV-2 antibodies and protective role of pre-existing antibodies to seasonal human coronaviruses on COVID-19. 2021:2021.02.22.21252150.
25. Ladner JT, Henson SN, Boyle AS, Engelbrektson AL, Fink ZW, Rahee F, et al. Epitope-resolved profiling of the SARS-CoV-2 antibody response identifies cross-reactivity with endemic human coronaviruses. Cell reports Medicine. 2021;2(1):100189.
26. Ng KW, Faulkner N, Cornish GH, Rosa A, Harvey R, Hussain S, et al. Preexisting and de novo humoral immunity to SARS-CoV-2 in humans. Science (New York, NY). 2020;370(6522):1339-43.
27. Yang R, Lan J, Huang B, A R, Lu M, Wang W, et al. Lack of antibody-mediated cross-protection between SARS-CoV-2 and SARS-CoV infections. EBioMedicine. 2020;58:102890.
28. Lv H, Wu NC, Tsang OT, Yuan M, Perera R, Leung WS, et al. Cross-reactive Antibody Response between SARS-CoV-2 and SARS-CoV Infections. Cell reports. 2020;31(9):107725.
29. Zhu Y, Yu D, Han Y, Yan H, Chong H, Ren L, et al. Cross-reactive neutralization of SARS-CoV-2 by serum antibodies from recovered SARS patients and immunized animals. Science advances. 2020;6(45).
30. Lipsitch M, Grad YH, Sette A, Crotty S. Cross-reactive memory T cells and herd immunity to SARS-CoV-2. Nature reviews Immunology. 2020;20(11):709-13.
31. Sumbul B, Sumbul HE, Okyay RA, Gülümsek E, Şahin AR, Boral B, et al. Is there a link between pre-existing antibodies acquired due to childhood vaccinations or past infections and COVID-19? A case control study. PeerJ. 2021;9:e10910.
32. Majdoubi A, Michalski C, O'Connell SE, Dada S, Narpala SR, Gelinas JP, et al. A majority of uninfected adults show pre-existing antibody reactivity against SARS-CoV-2. JCI insight. 2021.
33. Sette A, Crotty S. Pre-existing immunity to SARS-CoV-2: the knowns and unknowns. Nature reviews Immunology. 2020;20(8):457-8.
34. Tso FY, Lidenge SJ, Peña PB, Clegg AA, Ngowi JR, Mwaiselage J, et al. High prevalence of pre-existing serological cross-reactivity against severe acute respiratory syndrome coronavirus-2 (SARS-CoV-2) in sub-Saharan Africa. International journal of infectious diseases : IJID : official publication of the International Society for Infectious Diseases. 2021;102:577-83.

35. Lee CH, Pinho MP, Buckley PR, Woodhouse IB, Ogg G, Simmons A, et al. Potential CD8+ T Cell Cross-Reactivity Against SARS-CoV-2 Conferred by Other Coronavirus Strains. Frontiers in immunology. 2020;11:579480.
36. Freeman B, Lester S, Mills L, Rasheed MAU, Moye S, Abiona O, et al. Validation of a SARS-CoV-2 spike protein ELISA for use in contact investigations and sero-surveillance. 2020:2020.04.24.057323.
37. Post N, Eddy D, Huntley C, van Schalkwyk MCI, Shrotri M, Leeman D, et al. Antibody response to SARS-CoV-2 infection in humans: A systematic review. PloS one. 2020;15(12):e0244126.
38. Reche PA. Potential Cross-Reactive Immunity to SARS-CoV-2 From Common Human Pathogens and Vaccines. Frontiers in immunology. 2020;11:586984.
39. Doshi P. Covid-19: Do many people have pre-existing immunity? 2020;370:m3563.
40. Steiner S, Sotzny F, Bauer S, Na I-K, Schmueck-Henneresse M, Corman VM, et al. HCoV- and SARS-CoV-2 Cross-Reactive T Cells in CVID Patients. 2020;11(3347).
41. Mateus J, Grifoni A, Tarke A, Sidney J, Ramirez SI, Dan JM, et al. Selective and cross-reactive SARS-CoV-2 T cell epitopes in unexposed humans. 2020;370(6512):89-94.
42. Grifoni A, Weiskopf D, Ramirez SI, Mateus J, Dan JM, Moderbacher CR, et al. Targets of T Cell Responses to SARS-CoV-2 Coronavirus in Humans with COVID-19 Disease and Unexposed Individuals. Cell. 2020;181(7):1489-501.e15.
43. Braun J, Loyal L, Frentsch M, Wendisch D, Georg P, Kurth F, et al. SARS-CoV-2-reactive T cells in healthy donors and patients with COVID-19. Nature. 2020;587(7833):270-4.
44. Kim H, Seiler P, Jones JC, Ridout G, Camp KP, Fabrizio TP, et al. Antibody Responses to SARS-CoV-2 Antigens in Humans and Animals. Vaccines. 2020;8(4).
45. Anderson EM, Goodwin EC, Verma A, Arevalo CP, Bolton MJ, Weirick ME, et al. Seasonal human coronavirus antibodies are boosted upon SARS-CoV-2 infection but not associated with protection. Cell. 2021;184(7):1858-64.e10.
46. Song G, He W-t, Callaghan S, Anzanello F, Huang D, Ricketts J, et al. Cross-reactive serum and memory B-cell responses to spike protein in SARS-CoV-2 and endemic coronavirus infection. Nature Communications. 2021;12(1):2938.
47. Fraley E, LeMaster C, Banerjee D, Khanal S, Selvarangan R, Bradley T. Cross-reactive antibody immunity against SARS-CoV-2 in children and adults. Cellular & molecular immunology. 2021:1-3.
48. Nguyen-Contant P, Embong AK, Kanagaiah P, Chaves FA, Yang H, Branche AR, et al. S Protein-Reactive IgG and Memory B Cell Production after Human SARS-CoV-2 Infection Includes Broad Reactivity to the S2 Subunit. mBio. 2020;11(5).
49. Zhao Q, Elson CO. Adaptive immune education by gut microbiota antigens. Immunology. 2018;154(1):28-37.
50. Bradt V, Malafa S, von Braun A, Jarmer J, Tsouchnikas G, Medits I, et al. Pre-existing yellow fever immunity impairs and modulates the antibody response to tick-borne encephalitis vaccination. NPJ vaccines. 2019;4:38.
51. Pinto D, Sauer MM, Czudnochowski N, Low JS, Tortorici MA, Housley MP, et al. Broad betacoronavirus neutralization by a stem helix-specific human antibody. Science (New York, NY). 2021.
52. Lee IC, Huo TI, Huang YH. Gastrointestinal and liver manifestations in patients with COVID-19. Journal of the Chinese Medical Association : JCMA. 2020;83(6):521-3.
53. Jin X, Lian JS, Hu JH, Gao J, Zheng L, Zhang YM, et al. Epidemiological, clinical and virological

characteristics of 74 cases of coronavirus-infected disease 2019 (COVID-19) with gastrointestinal symptoms. Gut. 2020;69(6):1002-9.

54. Mao R, Qiu Y, He JS, Tan JY, Li XH, Liang J, et al. Manifestations and prognosis of gastrointestinal and liver involvement in patients with COVID-19: a systematic review and meta-analysis. The lancet Gastroenterology & hepatology. 2020;5(7):667-78.

55. Fan W, Wan Y, Li Q. Interleukin-21 enhances the antibody avidity elicited by DNA prime and MVA boost vaccine. Cytokine. 2020;125:154814.

56. Lu S, Manning S, Arthos J. Antigen engineering in DNA immunization. Methods in molecular medicine. 2000;29:355-74.

57. Nie J, Li Q, Wu J, Zhao C, Hao H, Liu H, et al. Establishment and validation of a pseudovirus neutralization assay for SARS-CoV-2. Emerging microbes & infections. 2020;9(1):680-6.

58. Li Q, Wu J, Nie J, Zhang L, Hao H, Liu S, et al. The Impact of Mutations in SARS-CoV-2 Spike on Viral Infectivity and Antigenicity. Cell. 2020;182(5):1284-94.e9.

59. Ren Y, Wang N, Hu W, Zhang X, Xu J, Wan Y. Successive site translocating inoculation potentiates DNA/recombinant vaccinia vaccination. Scientific reports. 2015;5:18099.

869 **Figure legends**

870

871 **Figure 1. Pre-existing cross-reactive antibodies against SARS-CoV-2 S**
872 **protein observed in both healthy human and naïve SPF mice**
873 **predominantly targeted S2**

874 The pre-existing cross-reactive antibodies against S1 and S2 were measured
875 using an in-house ELISA (Sample dilution factor: 100). (**A**) Plasma samples of
876 healthy individuals collected in 2020 (n=95). (**B**) Plasma samples of healthy
877 individuals collected in 2016 (n=78). (**C**) Sera of naïve C56BL/6J mice (n=12).
878 (**D**) Sera of naïve BALB/c mice (n=101). The dot lines showed the threshold of
879 background (3 folds of the background OD). Statistical analyses were
880 performed using the method of paired t-test.

881

882 **Figure 2 The pre-existing S protein binding antibodies in naïve SPF mice**
883 **recognized S2 exclusively and a dominant linear antibody epitope was**
884 **identified on the connector domain**

885 The pre-existing S1 and S2 cross-reactive antibody levels of 6 mice selected
886 for WB assays were shown in (**A**). (**B**) Western-blotting assays of pre-existing
887 cross-reactive antibodies for 6 selected mouse serum samples. The purities of
888 S1 and S2 proteins were shown by coomassie blue staining. (**C**) The minimal
889 epitope of P144 was defined using a method of competitive ELISA (Data
890 shown as mean±SD, n=5). Purified S2 protein was used as the coating antigen
891 and truncated peptides derived from P144 were used as competitors. The
892 decreases of competitive inhibition reflected the necessity of each amino acid
893 for the epitope recognition. Statistical differences among groups was analyzed
894 using One-way ANOVA. ****, P<0.0001. M: molecular weight markers; SP,
895 signal peptide; RBD, receptor-binding domain; FP, fusion peptide; HR, heptad
896 repeat; CH, central helix; CD, connector domain; TM, transmembrane domain;
897 CT, cytoplasmic tail.

898

899 **Figure 3 Cross-reactive antibodies recognizing epitope P144 widely**
900 **existed in both healthy human and naïve SPF mice**

901 P144 specific binding antibodies were detected using a method of competitive
902 ELISA. (**A**) For the detections of P144 specific binding antibodies in naïve SPF
903 mice, purified S2 protein was used as the coating antigen and P144 peptide

904 was used as the competitor. (**B**) For the detections of P144 specific binding
905 antibodies in healthy individuals, purified BSA-P144 conjugate was used as
906 the coating antigen and P144 peptide was used as the competitor. In both
907 experiments, the reduction of OD value reflected the presence of P144 binding
908 antibodies.

909

910 **Figure 4 The generation of the pre-existing S2 cross-reactive antibodies**
911 **were associated with commensal gut microbiota**
912 (**A**) Comparison of the levels of S2 specific pre-existing antibodies between
913 naïve mice maintained under SPF condition and mice in a sterile isolation pack.
914 (**B**) Comparison of commensal gut bacteria compositions between mice
915 housed in a SPF facility and mice in a sterile isolation pack by metagenomic
916 sequencing. Differences of bacterial abundance was analyzed by linear
917 discriminant analysis (LDA) analysis and shown as the histogram of LDA
918 scores. It was considered a significant effect size with LDA score > 4.0. (p),
919 Phylum. (c), Class. (o), Order. (f), Family. (g), Genus. (s), Species. **(C)**
920 Schematic overview of the fecal bacteria transplantation (n=6). The mice bred
921 in the isolation pack were treated with a mixture of ampicillin (1g/L),
922 metronidazole (0.5g/L), vancomycin (0.5g/L) and gentamycin (0.5g/L)
923 dissovled in drinking water supplemented with D-glucose (36.8g/L) for 14 days.
924 Two weeks after antibiotic treatment, fecal bacteria were freshly prepared from
925 SPF mice and delivered via oral gavage. **(D)** P144 specific antibody was
926 determined using an in-house ELISA method. Data are shown as mean±SD
927 (n=6). Statistical analyses were performed by the method of paired t-test.

928

929 **Figure 5 P144 specific monoclonal antibodies isolated from naïve SPF**
930 **mice cross-reacted with commensal gut bacteria from both human and**
931 **mouse**

932 Cross-reactivities between P144 specific mAbs and gut microbial antigens
933 were detected using WB assays. A purified mouse IgG was used as the control.
934 (**A**) WB assays of mouse fecal bacteria samples. L: mixed fecal bacteria
935 samples collected from 3 mice with low levels of pre-existing S2 binding
936 antibodies ($OD_{450nm-630nm} \leqslant 0.140$ at serum dilution of 1:100); H: mixed fecal
937 bacteria samples collected from 3 mice with high levels of pre-existing S2

938 binding antibodies ($OD_{450nm-630nm} \geqslant 0.615$ at serum dilution of 1:100). (**B**) WB
939 assays of fecal bacteria samples collected from 7 healthy individuals (Lanes
940 1-7). All the mAbs and the control mouse IgG were diluted at the final
941 concentration of 1μg/ml. Black arrows indicated the locations of protein bands
942 chosen for the Mass spectrometry analysis.

943

944 **Figure 6 Impact of pre-existing antibodies on the humoral immune**
945 **responses elicited by a DNA vaccine encoding SARS-CoV-2 S protein**
946 (**A**) Schematic illustration of the vaccination regimen. 50μg of the candidate
947 DNA vaccine was injected intra muscularly into each mice at week 0, week 2
948 and week 4. Two weeks after the final vaccination, the mice was sacrificed for
949 the measurements of specific immune responses. (**B**) Periphral blood was
950 collected before immunization and levels of pre-existing S2 specific IgG were
951 compared among three groups of mice. (**C**) Comparisons of endpoint IgG titers
952 against S2 in the serum of mice measured at 2 weeks post the last
953 immunization. (**D**) Comparisons of P144 specific IgG titers in the serum of
954 mice as measured using BSA-P144 conjugate as the coating antigen. (**E**)
955 Comparisons of P144 specific binding antibody levels as determined using a
956 method of competitive ELISA. (**F**) Endpoint IgG titers against S1 measured at
957 2 weeks post the final vaccination. (**G**) Neutralizing antibody titers against
958 SARS-CoV-2 D614G pseudo-virus in serum of mice at 2 weeks post the final
959 immunization. The vaccination experiment was repeated twice with 6 mice for
960 each group. Data were shown as mean±SD. Statistical analyses were
961 performed by the method of one-way ANONVA.

962

963 **Figure 7 The impact of pre-existing antibody on the levels of specific IgG**
964 **and IgA in BALF after vaccination**
965 BALF was collected from each mouse after euthanasia. Specific IgG (A and B)
966 and IgA (C and D) against S1 or S2 were detected using in-house ELISA
967 methods. All the BALF samples were adjusted to the initial total protein
968 concentration of 51.9μg/ml. Data are shown as mean± SD. Statistical analyses
969 were performed by the method of one-way ANONVA.

970

971 **Figure 8 The impact of pre-existing antibody on the minimum epitope**
972 **recognition of P144 after vaccination.**

973 The minimal epitope recognized by mouse sera after vaccination were
974 analyzed using a method of competitive ELISA. Purified BSA-P144 conjugate
975 was used as the coating antigen and truncated peptides derived from P144
976 were used as the competitors. The decreases of competitive inhibition
977 reflected the necessity of each amino acid for the epitope recognition.
978 Statistical analyses were performed by the method of two-tailed t-test (*, $P<$
979 0.05, **, $P<0.01$, ***, $P<0.001$).
980
981 **Figure 9 The impact of pre-existing antibody on the cellular immune**
982 **responses after vaccination**
983 (**A**) The diagram of the method for cellular immune responses assays. (**B**) S1
984 and S2 specific IFN-γ responses were compared among groups of mice with
985 different levels of pre-existing S2 cross-reactive antibodies. Additionally, S1 (**C**)
986 and S2 (**D**) specific releases of IL-2, IL-6 and TNF-α as measured using the
987 method of multiplex cytokine bead assay were also compared among different
988 groups. Data were shown as mean$\pm$ SD. SFU, spot forming units.
989
990 **Figure 10 Levels of pre-existing S2 cross-reactive antibody correlated**
991 **with RBD binding antibody responses elicited by an inactivated**
992 **SARS-CoV-2 vaccine**
993 **(A)** Peripheral blood samples were collected from 28 healthy vaccinees who
994 received two doses of an inactivated SARS-CoV-2 vaccine at baseline and 14
995 days post 2nd dose, respectively. The RBD binding antibody titers were
996 measured by ELISA. The neutralizing antibody responses were quantified by a
997 commercialized surrogate virus neutralization test (sVNT) (Suzhou Sym-Bio
998 Life Science Co., Ltd). **(B and C**) Correlations between RBD binding antibody
999 titers and levels of pre-existing S2 or P144 specific IgG. **(D)** Correlation
1000 between neutralizing antibody concentrations and pre-existing P144 binding
1001 antibody levels. Statistical analyses were performed using the method of
1002 Spearman's correlation**.**
1003
1004
1005
1006
1007

1008 **Supplementary figures**

1009

1010 **Supplementary Figure 1 A dominant linear epitope recognized by the**
1011 **pre-existing antibodies was located on the connector domain of S2**
1012 (**A**) The location of P144 on the full length of SARS-CoV-2 spike protein.
1013 Synthesized peptides (18-mer, overlapped by 11amino acids) spanning the full
1014 length of S2 were divided into 9 peptide pools, each contained 8 peptides. To
1015 identify the potential antibody binding epitopes, we first performed competitive
1016 ELISA assays using the peptide pools as competitors (Data not shown). The
1017 pool showing significant inhibition effect was further delineated by testing the
1018 inhibiting efficiencies of each individual peptides (**B**).The data was shown as
1019 mean±SD, n=5. Inhibition efficiencies among groups were analyzed using the
1020 method of One-way ANOVA. ****, $p<0.0001$. SP, signal peptide; RBD,
1021 receptor-binding domain; FP, fusion peptide; HR, heptad repeat; CH, central
1022 helix; CD, connector domain; TM, transmembrane domain; CT, cytoplasmic
1023 tail.

1024

1025 **Supplementary Figure 2 Phylogenetic analysis of the spike protein**
1026 **sequences of major human coronaviruses**
1027 The sequences of SARS-CoV-2 Wuhan (YP_009724390), MERS-CoV
1028 (QFQ59587.1), HCoV-OC43 (QDH43719.1), HCoV-NL63 (AKT07952),
1029 HCoV-229E (AOG74783.1) and HCoV-HKU1 (YP_173238) were retrieved
1030 from NCBI database. The sequences of B.1.1.7, D614G, B.1.351, B.1.525,
1031 B.1.617 and P.1(B.1.1.281) were obtained from Global Initiative on Sharing
1032 Avian Influenza Data (GISAID). Boxed fragments represent IEDB predicted
1033 linear antibody epitope (http://tools.iedb.org/bcell/).

1034

1035 **Supplementary Figure 3 Evidences that implied the link between**
1036 **pre-existing S2 cross-reactive antibodies and commensal gut bacteria**
1037 (**A**) Principle component analysis (PCA) of gut microbial communities between
1038 4 mice in SPF condition and 4 mice in a sterile isolation pack. (**B**) The
1039 splenocytes and lymphocytes of MLN were harvested from 4 naive C57BL/6J
1040 mice with relatively high levels of pre-existing S2 cross-reactive antibodies. S2
1041 specific B cells were defined as $CD45^{+}CD19^{+}S2^{+}$ (Left). Statistical analysis
1042 was performed by the method of paired t-test (Right).

1043

1044 **Supplementary Figure 4 Characterizations of the minimal epitope**
1045 **recognitions for the 6 monoclonal antibodies isolated from naïve mice**
1046 Six P144 specific monoclonal antibodies were isolated from 2 naïve SPF mice
1047 using the hybridoma technology. (**A**) The minimum epitope recognitions of
1048 clones H9, E10, G13, F5 and G18 were similar detected by a method of
1049 competitive ELISA. Purified S2 protein was used as the coating antigen and
1050 the truncated peptides derived from P144 were used as the competitors. (**B**)
1051 The epitope recognition of clone M3 was analyzed using purified S2 protein as
1052 the coating antigen and each listed peptide was used as the competitor. SP,
1053 signal peptide; RBD, receptor-binding domain; FP, fusion peptide; HR, heptad
1054 repeat; CH, central helix; CD, connector domain; TM, transmembrane domain;
1055 CT, cytoplasmic tail.
1056

1057 **Supplementary Figure 5 Neutralizing activities of the purified monoclonal**
1058 **antibodies as measured using a pseudo virus neutralization assay**
1059 Neutralization activities of 6 isolated mAbs against 5 major SARS-CoV-2
1060 variants (D614G, B.1.617, B.1.1.7, B.1.351 and P.1) were examined using a
1061 pseudo virus neutralization assay. Purified mouse IgG was used as negative
1062 control and serum of an RBD protein vaccinated goat was use as positive
1063 control. Purified mAbs and control mouse IgG were tested at a concentration
1064 of 1μg/ml; positive goat serum was diluted at 1:90.
1065

1066 **Supplementary Figure 6 Validation of cross-reactivity between P144**
1067 **specific mAb and *E. coli***
1068 Proteins in the WCL of *E. coli* (strain DH5α) were separated by SDS-PAGE.
1069 The cross-reactivity between *E. coli* and P144 specific mAb (clone F5) was
1070 determined by western blotting. F5 or a purified mouse IgG was used as the
1071 first antibody at the concentration of 1 μg/ml. Black arrows pointed out the
1072 bands with MWs equal to *E. coli* proteins identified by LCMS analysis.
1073

Figures and Figure legends

Figure 1

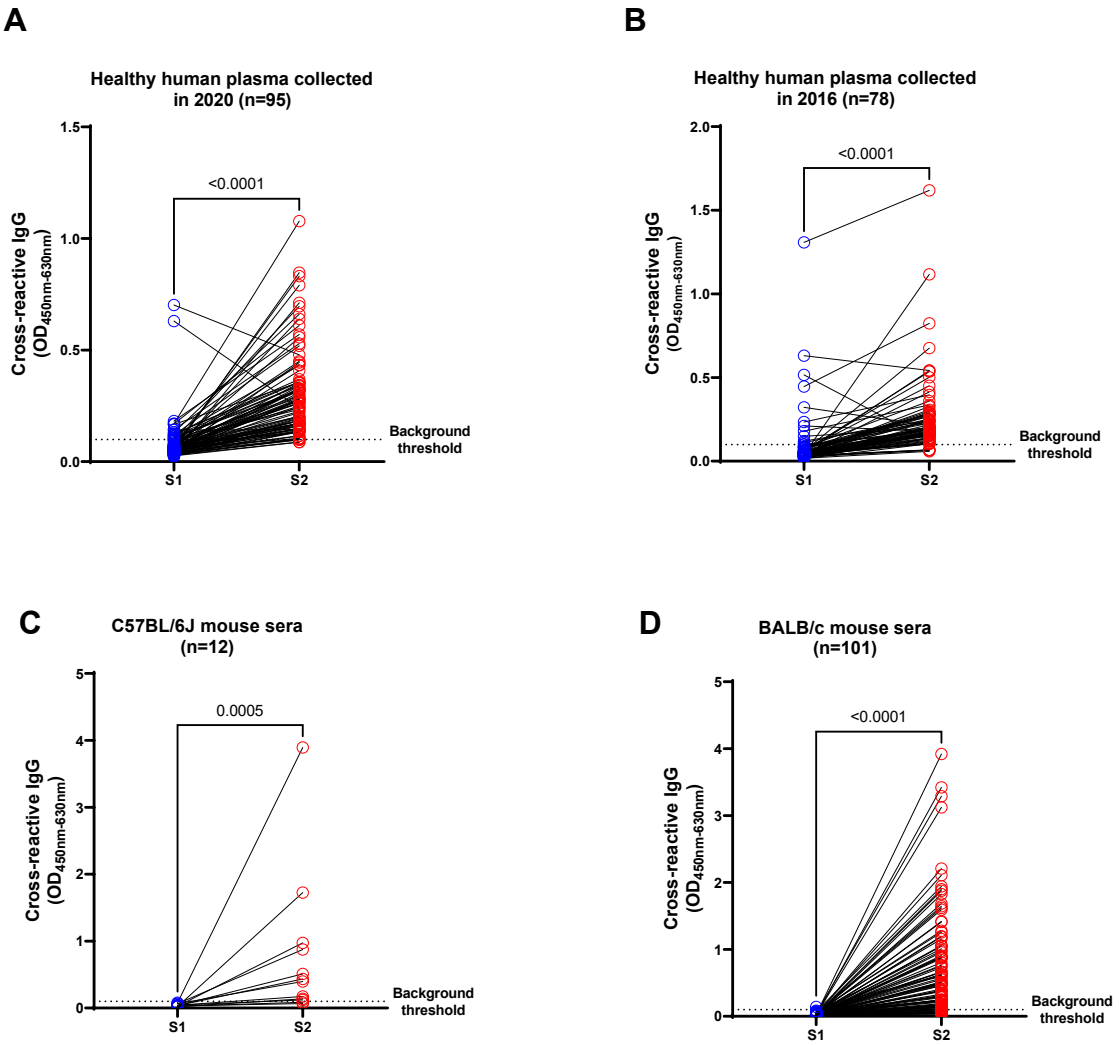

Figure 1. Pre-existing cross-reactive antibodies against SARS-CoV-2 S protein observed in both healthy human and naïve SPF mice predominantly targeted S2 subunit. The pre-existing cross-reactive antibodies against S1 and S2 were measured using an in-house ELISA (Sample dilution factor: 100). (**A**) Plasma samples of healthy individuals collected in 2020 (n=95). (**B**) Plasma samples of healthy individuals collected in 2016 (n=78). (**C**) Sera of naïve C57BL/6J mice (n=12). (**D**) Sera of naïve BALB/c mice (n=101). The dot lines showed the threshold of background (3 folds of the background OD). Statistical analyses were performed using the method of paired t-test.

Figure 2

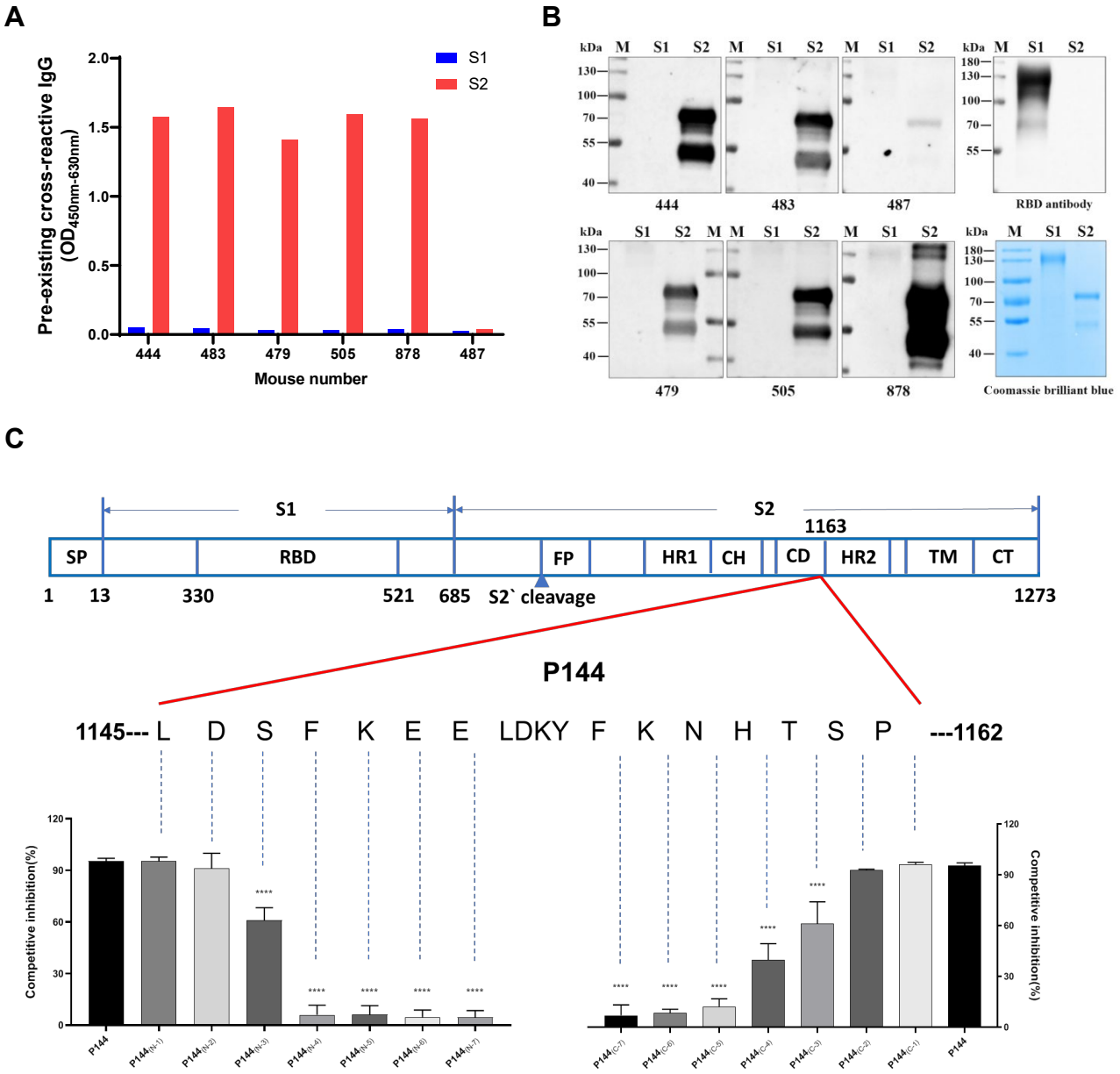

Figure 2. The pre-existing S protein binding antibodies in naïve SPF mice recognized S2 exclusively and a dominant linear antibody epitope was identified on the connector domain. The pre-existing S1 and S2 cross-reactive antibody levels of 6 mice selected for WB assays were shown in (**A**). (**B**) Western-blotting assays of pre-existing cross-reactive antibodies for 6 selected mouse serum samples. The purities of S1 and S2 proteins were shown by coomassie blue staining. (**C**) The minimal epitope of P144 was defined using a method of competitive ELISA (Data shown as mean±SD, n=5). Purified S2 protein was used as the coating antigen and truncated peptides derived from P144 were used as competitors. The decreases of competitive inhibition reflected the necessity of each amino acid for the epitope recognition. Statistical differences among groups was analyzed using One-way ANOVA. ****, P<0.0001. M: molecular weight markers; SP, signal peptide; RBD, receptor-binding domain; FP, fusion peptide; HR, heptad repeat; CH, central helix; CD, connector domain; TM, transmembrane domain; CT, cytoplasmic tail.

Figure 3

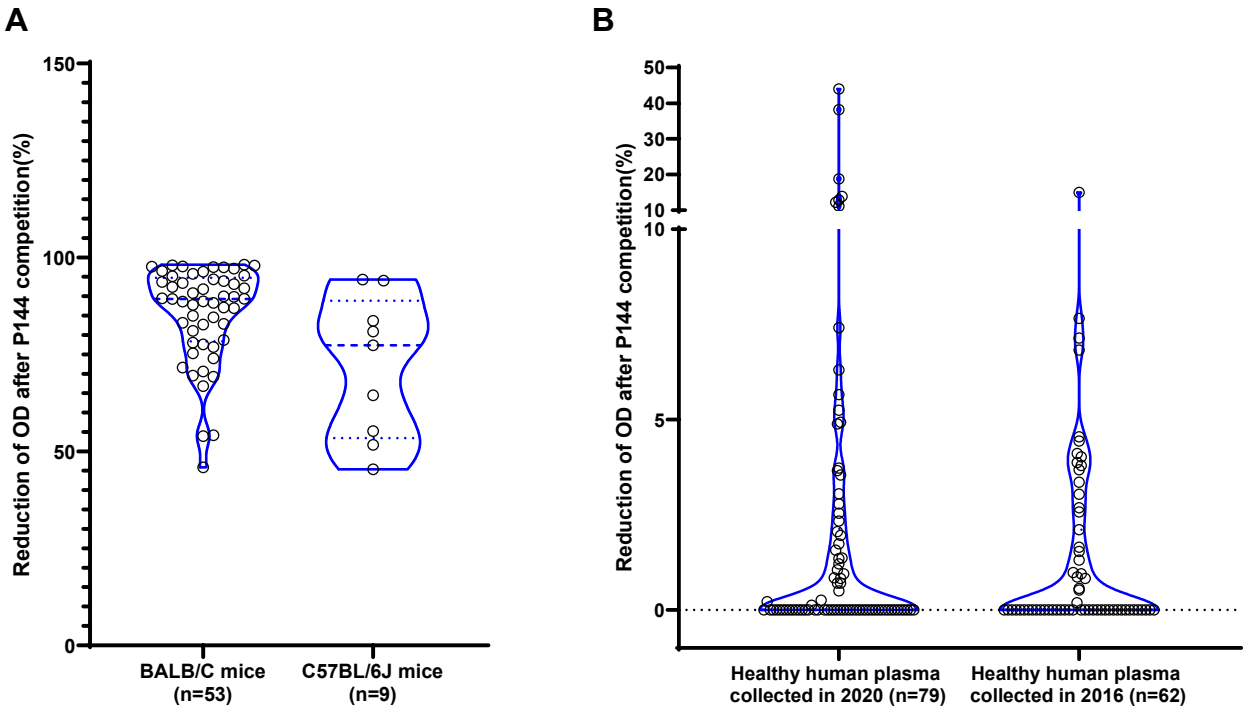

Figure 3. Cross-reactive antibodies recognizing epitope P144 widely existed in both healthy human and naïve SPF mice. P144 specific binding antibodies were detected using a method of competitive ELISA. (**A**) For the detections of P144 specific binding antibodies in naïve SPF mice, purified S2 protein was used as the coating antigen and P144 peptide was used as the competitor. (**B**) For the detections of P144 specific binding antibodies in healthy individuals, purified BSA-P144 conjugate was used as the coating antigen and P144 peptide was used as the competitor. In both experiments, the reduction of OD value reflected the presence of P144 binding antibodies.

Figure 4

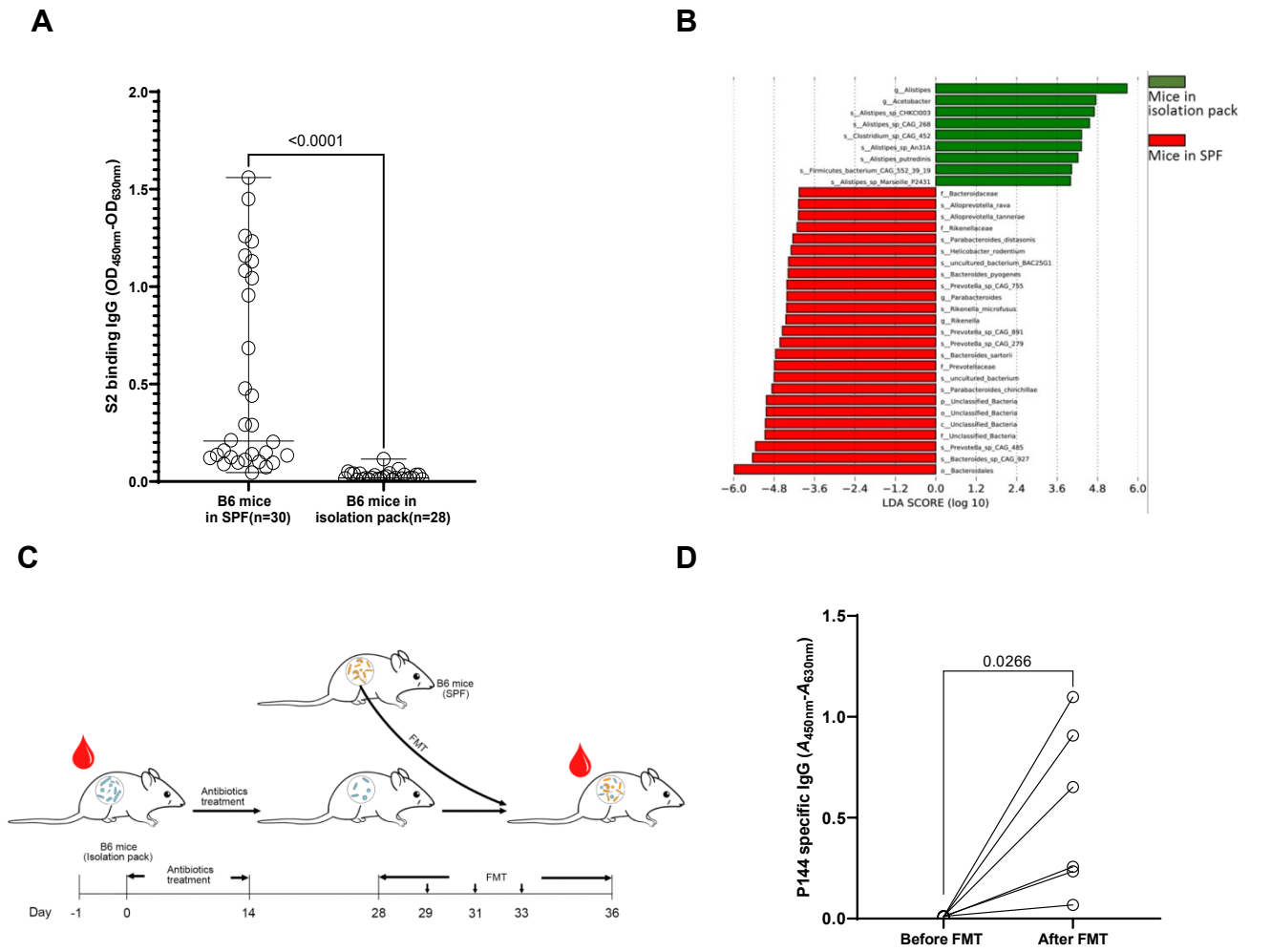

Figure 4. The generation of the pre-existing S2 cross-reactive antibodies might be associated with commensal gut microbiota. (**A**) Comparison of the levels of S2 specific pre-existing antibodies between naïve mice maintained under SPF condition and mice in a sterile isolation pack. (**B**) Comparison of commensal gut bacteria compositions between mice housed in a SPF facility and mice in a sterile isolation pack by metagenomic sequencing. Differences of bacterial abundance was analyzed by linear discriminant analysis (LDA) analysis and shown as the histogram of LDA scores. It was considered a significant effect size with LDA score > 4.0. (p), Phylum. (c), Class. (o), Order. (f), Family. (g), Genus. (s), Species. **(C and D)** P144 specific antibodies were induced in mice bred in the isolation pack after being transplanted with fecal bacteria isolated from SPF mice. **(C)** Schematic overview of the fecal bacteria transplantation (n=6). The mice bred in the isolation pack were treated with a mixture of ampicillin (1g/L), metronidazole (0.5g/L), vancomycin (0.5g/L) and gentamycin (0.5g/L) in drinking water supplemented with D-glucose (36.8g/L) for 14 days. Two weeks after antibiotic treatment, fecal bacteria were freshly prepared from SPF mice and delivered via oral gavage. **(D)** For the detections of P144 cross-reactive antibodies, purified BSA-P144 conjugate was used as the coating antigen and specific binding antibody was determined using an in-house ELISA method. Data are shown as mean±SD. Statistical analyses were performed by the method of paired t-test.

Figure 5

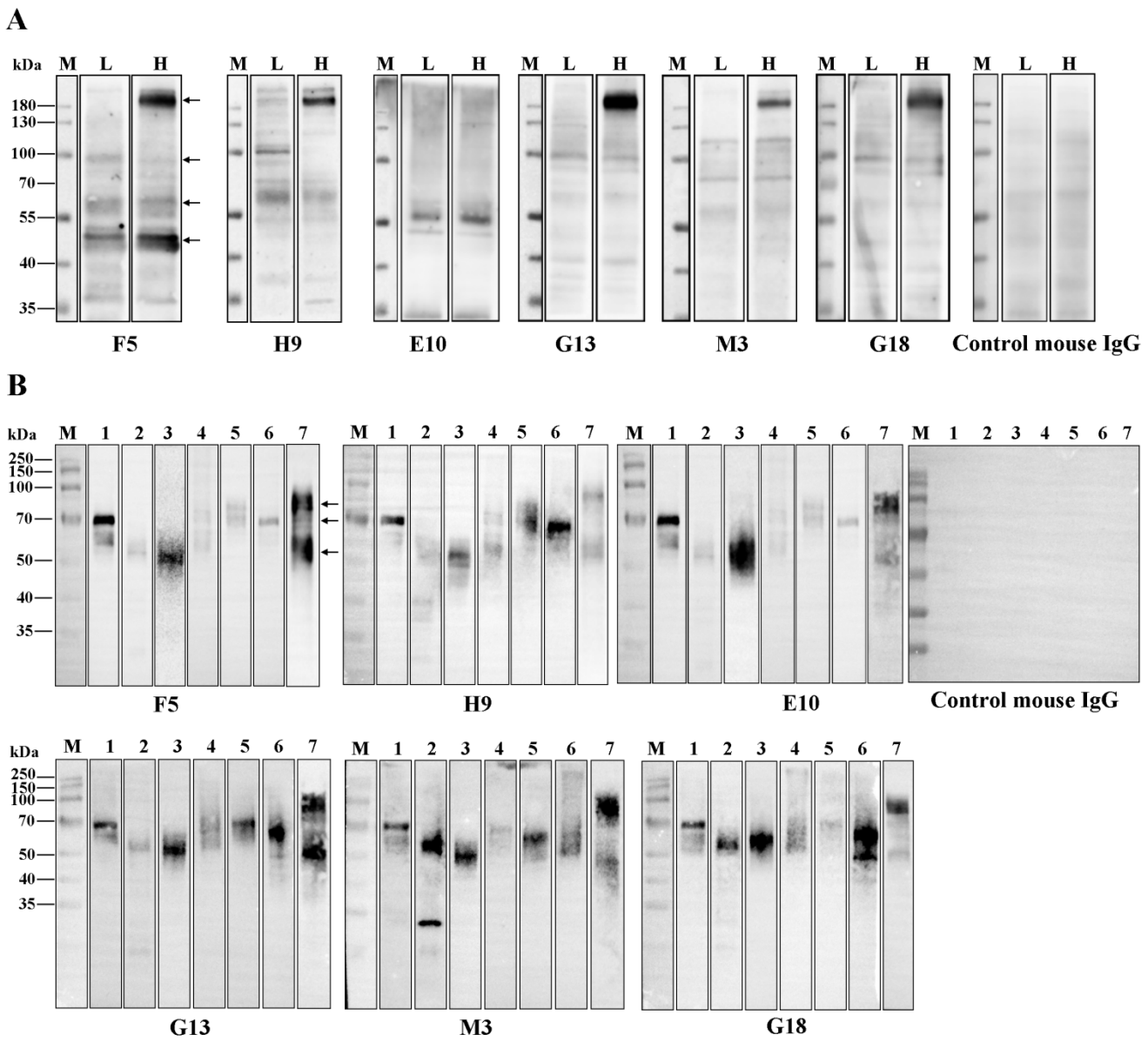

Figure 5. P144 specific monoclonal antibodies isolated from naïve SPF mice cross-reacted with commensal gut bacteria from both human and mouse. Cross-reactivities between P144 specific mAbs and gut microbial antigens were detected using WB assays. A purified mouse IgG was used as the control. (**A**) WB assays of mouse fecal bacteria samples. L: mixed fecal bacteria samples collected from 3 mice with low levels of pre-existing S2 binding antibodies ($OD_{450nm-630nm}$≤0.140 at serum dilution of 1:100); H: mixed fecal bacteria samples collected from 3 mice with high levels of pre-existing S2 binding antibodies ($OD_{450nm-630nm}$≥0.615 at serum dilution of 1:100). (**B**) WB assays of fecal bacteria samples collected from 7 healthy individuals (Lanes 1-7). All the mAbs and the control mouse IgG were diluted at the final concentration of 1μg/ml. Black arrows indicated the locations of protein bands chosen for the Mass spectrometry analysis.

Figure 6

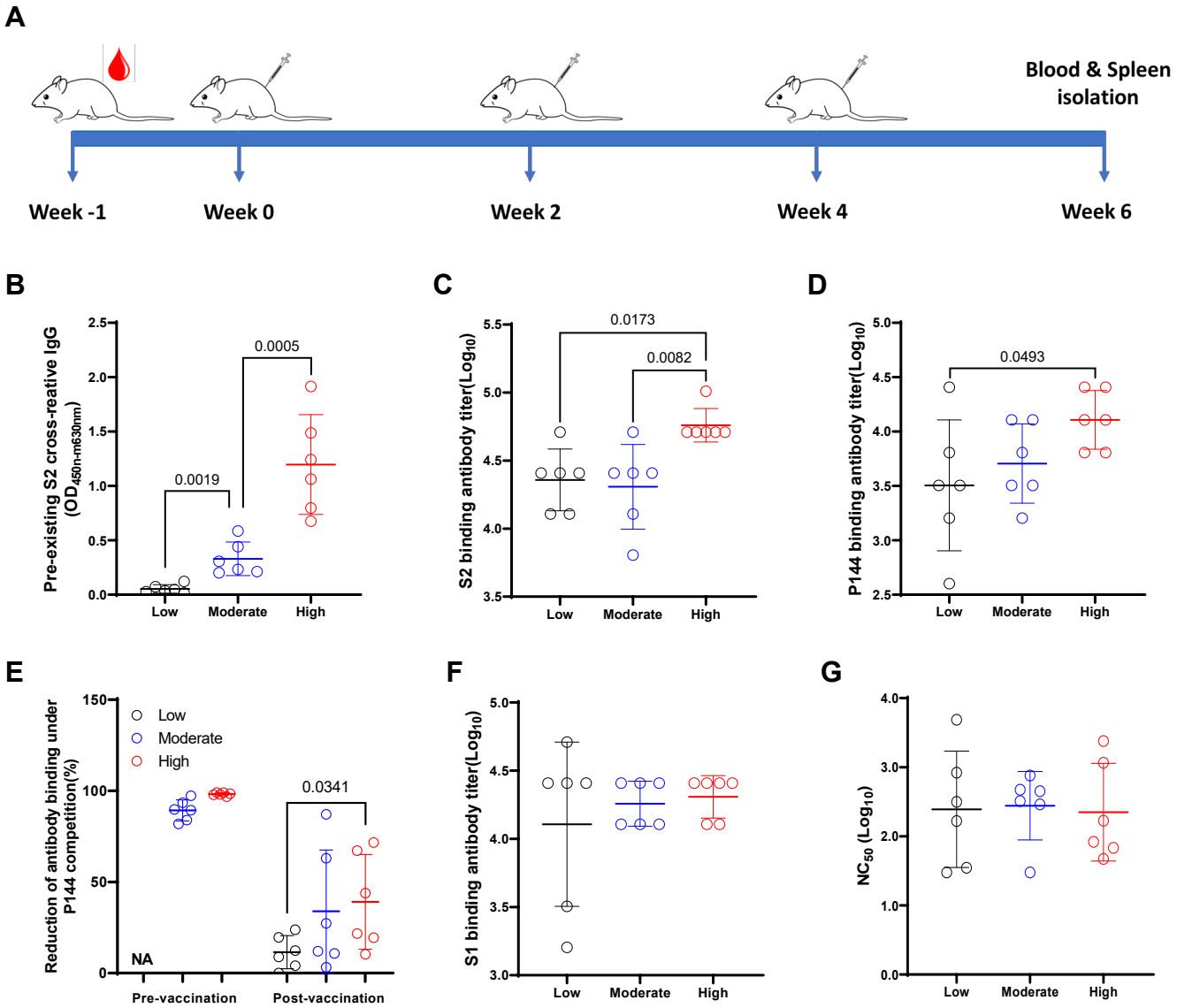

Figure 6. Impact of pre-existing antibodies on the humoral immune responses elicited by a DNA vaccine encoding SARS-CoV-2 S protein. (**A**) Schematic illustration of the vaccination regimen. 50μg of the candidate DNA vaccine was injected intra muscularly into each mice at week 0, week 2 and week 4. Two weeks after the final vaccination, the mice was sacrificed for the measurements of specific immune responses. (**B**) Periphral blood was collected before immunization and levels of pre-existing S2 specific IgG were compared among three groups of mice. (**C**) Comparisons of endpoint IgG titers against S2 in the serum of mice measured at 2 weeks post the last immunization. (**D**) Comparisons of P144 specific IgG titers in the serum of mice as measured using BSA-P144 conjugate as the coating antigen. (**E**) Comparisons of P144 specific binding antibody levels as determined using a method of competitive ELISA. (**F**) Endpoint IgG titers against S1 measured at 2 weeks post the final vaccination. (**G**) Neutralizing antibody titers against SARS-CoV-2 D614G pseudo-virus in serum of mice at 2 weeks post the final immunization. The vaccination experiment was repeated twice with 6 mice for each group. Data were shown as mean±SD. Statistical analyses were performed by the method of one-way ANONVA.

Figure 7

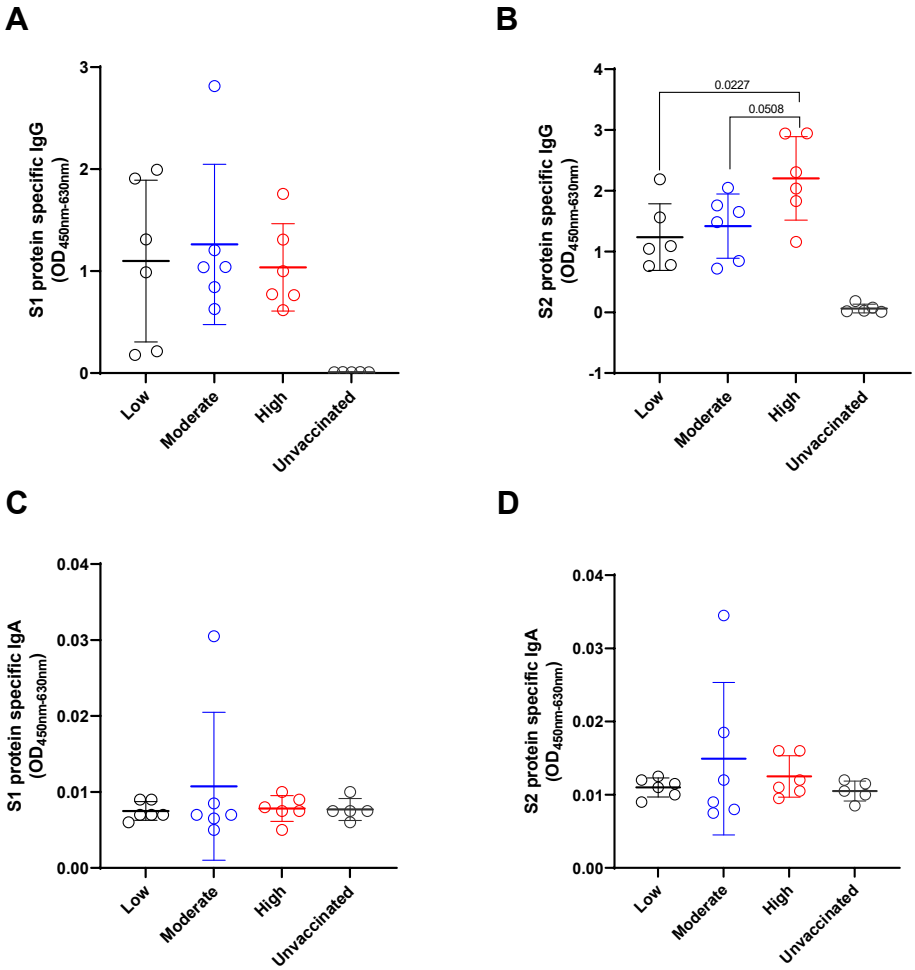

Figure 7. The impact of pre-existing antibody on the levels of specific IgG and IgA in BALF after vaccination. BALF was collected from each mouse after euthanasia. Specific IgG (**A** and **B**) and IgA (**C** and **D**) against S1 or S2 were detected using in-house ELISA methods. All the BALF samples were adjusted to the initial total protein concentration of 51.9μg/ml. Data are shown as mean± SD. Statistical analyses were performed by the method of one-way ANOVA.

Figure 8

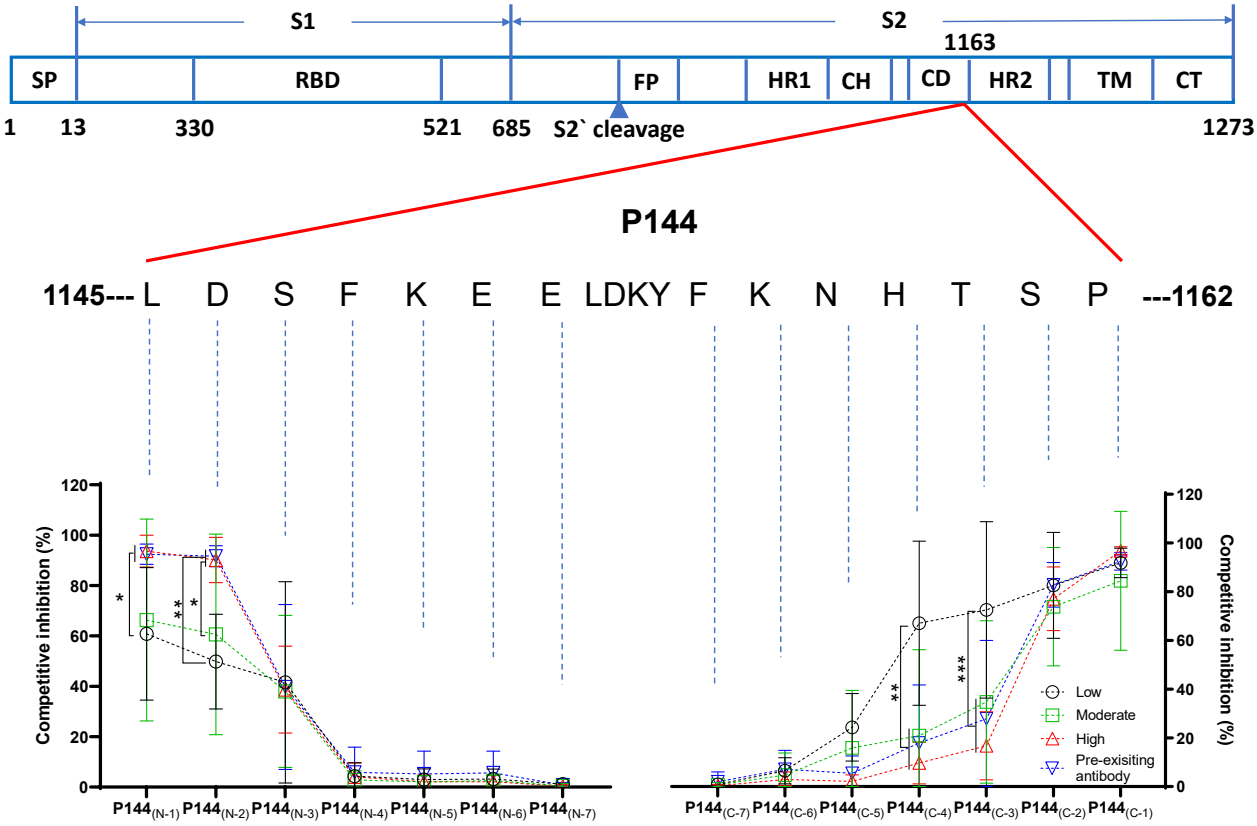

Figure 8. The impact of pre-existing antibody on the minimum epitope recognition of P144 after vaccination. The minimal epitope recognized by mouse sera after vaccination were analyzed using a method of competitive ELISA. Purified BSA-P144 conjugate was used as the coating antigen and truncated peptides derived from P144 were used as the competitors. The decreases of competitive inhibition reflected the necessity of each amino acid for the epitope recognition. Statistical analyses were performed by the method of two-tailed t-test (*, $P < 0.05$, **, $P < 0.01$, ***, $P < 0.001$).

Figure 9

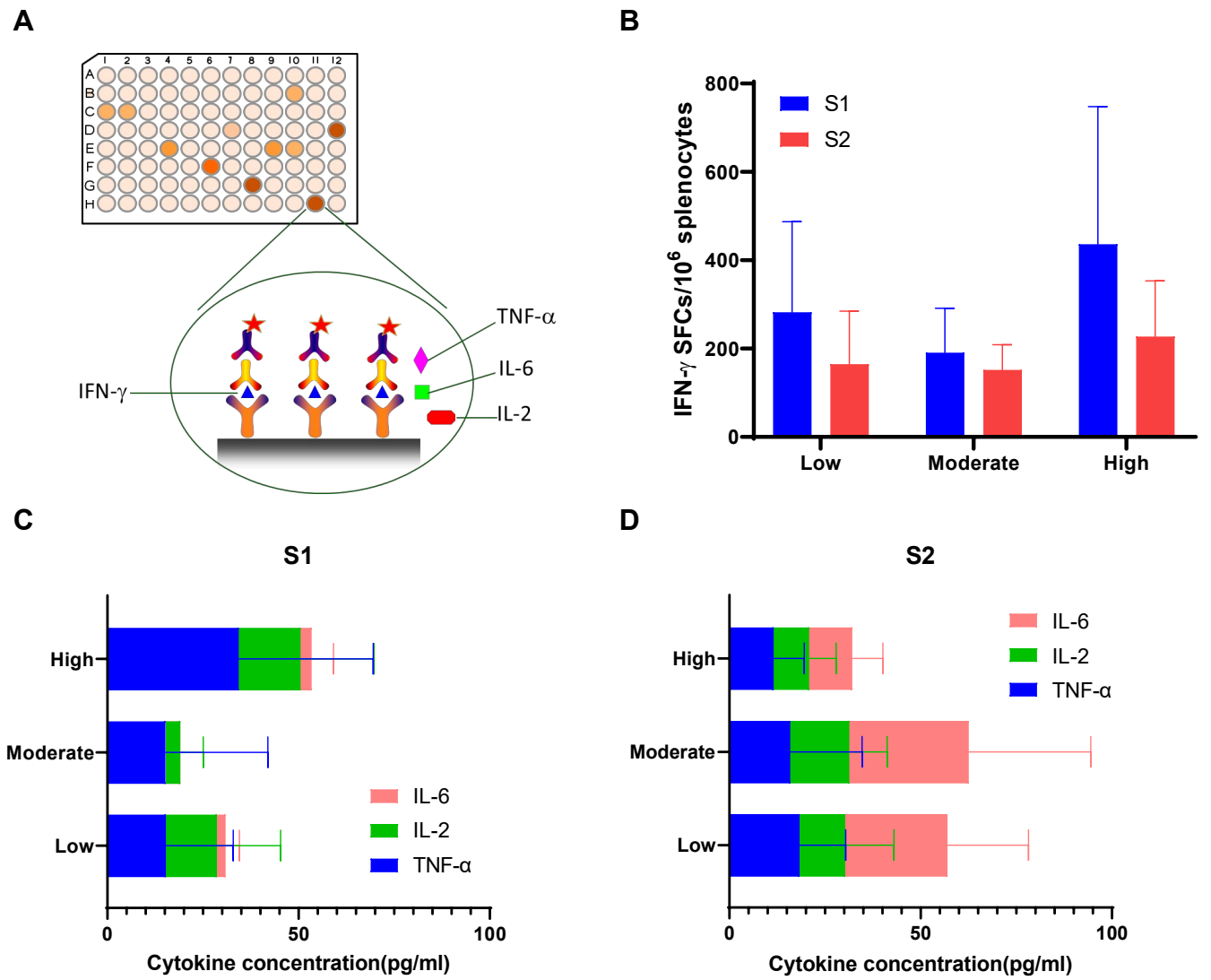

Figure 9. The impact of pre-existing antibody on the cellular immune responses after vaccination. (**A**) The diagram of the method for cellular immune responses assays. (**B**) S1 and S2 specific IFN-γ responses were compared among groups of mice with different levels of pre-existing S2 cross-reactive antibodies. Additionally, S1 (**C**) and S2 (**D**) specific releases of IL-2, IL-6 and TNF-α as measured using the method of multiplex cytokine bead assay were also compared among different groups. Data were shown as mean± SD. SFU, spot forming units.

Figure 10

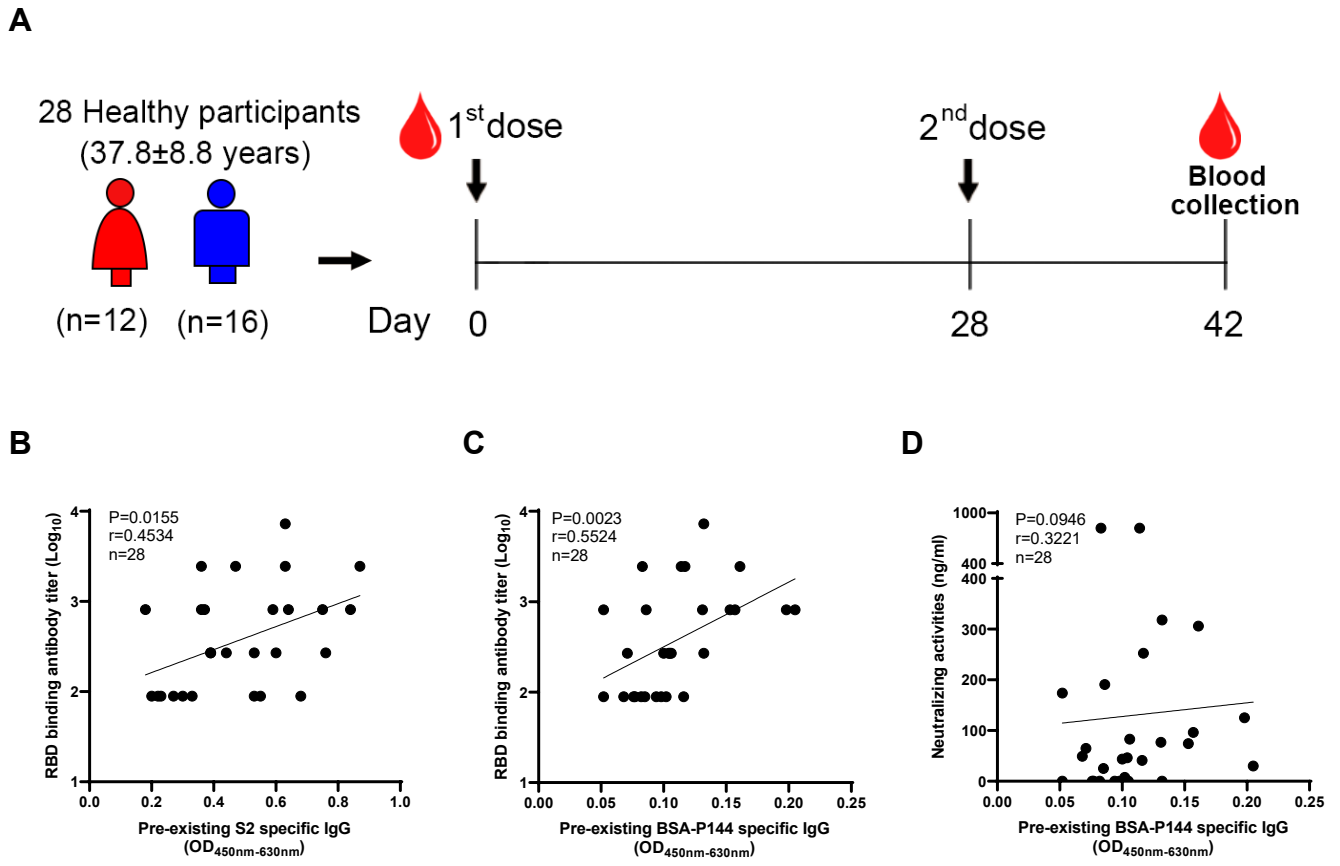

Figure 10. Correlation of pre-existing antibody with RBD and neutralizing activities in healthy individuals vaccinated with inactivated COVID19 vaccine (BBIBP-CorV). (A) 28 healthy individuals were selected and their plasma were collected both before and after vaccinated with inactivated COVID19 vaccine twice. The pre-existing P144 and pre-existing S2 specific antibody were evaluated in plasma before vaccination. The neutralization activities and RBD binding antibody titer were analyzed in plasma after vaccination. **(B and C**) Correlation between RBD binding antibody titer with pre-existing S2 specific IgG or pre-existing BSA-P144 specific IgG. **(D)** Correlation between neutralizing activities with pre-existing BSA-P144 specific IgG. All Correlation was statistically evaluated using Spearman's correlation and linear regression**.**

Table 1 Demographics of SARS-CoV-2 unexposed healthy individuals

Sample Collection Time	**2016**	**2020**
Number of individuals	78	95
Gender (males, females)	17, 61	78, 17
Age, years (mean ± SD)	35.88 ± 8.40	30.40 ± 7.55

Table 2 Potential cross-reactive antigens identified in mouse fecal bacteria

NCBI Accession #	Protein name	Bacterium	Score	Proteins	Unique Peptides	Peptides	PSMs	Area	MW [kDa]
Q8A470	DNA-directed RNA polymerase subunit beta' OS	Bacteroides thetaiotaomicron	168.01	550	2	6	6	3.536E7	158.3
Q5L897	DNA-directed RNA polymerase subunit beta OS	Bacteroides fragilis	92.15	8	2	3	3	8.315E6	142.4
Q8A1G1	TonB-dependent receptor SusC OS	Bacteroides thetaiotaomicron	145.74	1	1	2	3	1.385E8	111.1
Q46509	Aldehyde oxidoreductase OS	Desulfovibrio gigas	75.93	1	1	1	1	8.506E6	97.0
P22983	Pyruvate, phosphate dikinase OS	Clostridium symbiosum	109.83	7	2	2	2	3.721E7	96.6
P0A9Q8	Aldehyde-alcohol dehydrogenase OS	Escherichia coli	34.29	1	1	1	1	1.085E7	96.1
Q826F6	Chaperone protein dnaK2 OS	Streptomyces avermitilis	20.37	1	1	1	1	1.059E7	67.5
Q892R0	Chaperone protein DnaK OS	Clostridium tetani	51.52	5	1	1	1	1.780E7	66.4
B1I9W8	L-fucose isomerase OS	Streptococcus pneumoniae	57.33	12	2	2	2	2.792E7	65.7
P95334	Chaperone protein DnaK OS	Myxococcus xanthus	39.23	4	1	1	1	1.792E7	65.3
Q1MPZ9	Formate--tetrahydrofolate ligase OS	Lawsonia intracellularis	62.49	1	2	2	2	2.068E7	64.2
P26929	Urease subunit alpha OS	Lactobacillus fermentum	134.06	4	4	4	5	1.526E7	61.8
Q9I165	Periplasmic trehalase OS	Pseudomonas aeruginosa	77.05	1	1	1	1	4.240E8	61.1
Q9EZ02	Pyrophosphate--fructose 6-phosphate 1-phosphotransferase OS	Spirochaeta thermophila	68.21	2	1	1	1	1.192E7	61.0
P14407	Fumarate hydratase class I, anaerobic OS	Escherichia coli	30.79	1	1	1	1	6.580E6	60.1
Q189R2	Formate--tetrahydrofolate ligase OS	Clostridioides difficile	123.52	22	3	4	4	2.621E7	59.9
P22252	Flagellin B OS	Campylobacter jejuni subsp. jejuni serotype O:6	75.42	1	1	1	1	1.478E7	59.7
Q1WTW0	Formate--tetrahydrofolate ligase OS	Lactobacillus salivarius	83.43	23	1	1	1	5.229E7	59.4
A7HLZ4	Formate--tetrahydrofolate ligase OS	Fervidobacterium nodosum	93.49	29	1	2	2	8.036E6	59.2
C4ZBL1	Phosphoenolpyruvate carboxykinase (ATP) OS	Agathobacter rectalis	211.34	4	1	4	5	3.965E7	59.0
A6LFQ4	Phosphoenolpyruvate carboxykinase (ATP) OS	Parabacteroides distasonis	32.29	1	1	1	1	8.523E6	58.9
A3MZI4	Formate--tetrahydrofolate ligase OS	Actinobacillus pleuropneumoniae serotype 5b	78.45	78	1	2	2	1.320E8	58.9
Q2LPJ8	60 kDa chaperonin 1 OS	Syntrophus aciditrophicus	101.22	15	1	2	3	2.217E7	58.6
Q3ALZ3	60 kDa chaperonin 1 OS	Synechococcus sp.	113.34	23	1	2	3	9.973E7	58.5
B8J123	60 kDa chaperonin OS	Desulfovibrio desulfuricans	232.59	27	2	5	6	9.659E7	58.4
Q72AL6	60 kDa chaperonin OS	Desulfovibrio vulgaris	126.02	9	1	3	3	2.402E7	58.4

A0Q2T1	60 kDa chaperonin OS	Clostridium novyi	78.78	16	1	2	2	2.292E7	58.1
B0SCC0	60 kDa chaperonin OS	Leptospira biflexa serovar Patoc	49.58	1	1	1	1	1.882E8	58.1
B2TIX0	60 kDa chaperonin OS	Clostridium botulinum	126.34	35	1	3	3	4.903E7	57.9
A7GZ43	60 kDa chaperonin OS	Campylobacter curvus	105.05	41	2	3	3	5.327E7	57.9
Q67KB8	60 kDa chaperonin OS	Symbiobacterium thermophilum	107.47	126	1	3	3	9.411E7	57.9
B5YDR9	60 kDa chaperonin OS	Dictyoglomus thermophilum	59.61	2	1	1	1	3.345E7	57.9
Q3ADX3	60 kDa chaperonin OS	Carboxydothermus hydrogenoformans	104.07	25	1	2	3	7.715E7	57.6
O50305	60 kDa chaperonin OS	Bacillus halodurans	250.57	55	3	4	6	3.021E8	57.4
P26821	60 kDa chaperonin OS	Clostridium perfringens	131.27	36	1	3	3	4.609E7	57.3
P37282	60 kDa chaperonin OS	Lactococcus lactis subsp. lactis	102.15	18	1	2	2	4.298E7	57.2
C4ZD46	60 kDa chaperonin OS	Agathobacter rectalis	372.10	52	3	5	8	3.352E8	57.1
A6L8C4	Glucose-6-phosphate isomerase OS	Parabacteroides distasonis	88.85	55	1	2	3	5.392E8	48.7
P43793	NADP-specific glutamate dehydrogenase OS	Haemophilus influenzae	96.32	2	1	2	2	7.357E7	48.6
P00370	NADP-specific glutamate dehydrogenase OS	Escherichia coli	161.88	1	1	3	4	3.280E8	48.6
P15111	NADP-specific glutamate dehydrogenase OS	Salmonella typhimurium	185.28	4	1	4	5	1.755E8	48.5
P94316	NAD-specific glutamate dehydrogenase OS	Bacteroides fragilis	192.93	3	3	5	6	1.730E8	48.4
Q1WSY0	Enolase OS	Lactobacillus salivarius	79.89	8	3	3	3	1.340E7	48.0
B7MD95	Trigger factor OS	Escherichia coli O45:K1	78.80	10	2	2	2	4.344E7	47.8
B2GAM0	Enolase OS	Lactobacillus fermentum	79.94	8	2	2	2	1.858E7	47.8
Q6MEY2	Enolase OS	Protochlamydia amoebophila	112.67	1	1	1	1	7.493E7	47.5
Q0SNH5	Enolase OS	Borrelia afzelii	71.86	2	1	1	1	4.654E7	47.4
G3KIM4	Lactoyl-CoA dehydratase subunit alpha (Fragment) OS	Anaerotignum propionicum	63.03	1	1	1	1	1.136E7	47.4
Q9I3S1	Biofilm dispersion protein BdlA OS	Pseudomonas aeruginosa	59.07	22	1	1	1	3.282E7	46.9
B8J4A8	Sulfate adenylyltransferase OS	Desulfovibrio desulfuricans	210.65	1	5	5	5	2.656E7	46.9
A6L3M9	Enolase OS	Bacteroides vulgatus	48.62	2	1	2	2	3.004E7	46.7
Q043Z5	Enolase 1 OS	Lactobacillus gasseri	289.72	4	5	5	5	4.189E7	46.6
Q1ISS7	Enolase OS	Koribacter versatilis	71.57	4	1	1	1	7.884E6	46.5
B8DTI9	Enolase OS	Bifidobacterium animalis subsp. lactis	115.71	4	2	2	2	1.684E7	46.4
A7GUR7	Enolase OS	Bacillus cytotoxicus	122.68	17	2	2	3	2.771E7	46.4
Q2LR33	Enolase OS	Syntrophus aciditrophicus	31.73	1	1	1	1	4.823E7	46.2
Q89Z05	Enolase OS	Bacteroides thetaiotaomicron	140.16	2	2	4	5	3.005E7	46.1

B2RLL7	Enolase OS	Porphyromonas gingivalis	123.91	2	2	3	3	2.636E7	45.8
Q6MPQ2	Enolase OS	Bdellovibrio bacteriovorus	66.50	1	1	1	1	8.918E6	45.7
B0K742	Serine hydroxymethyltransferase OS	Thermoanaerobacter pseudethanolicus	85.67	92	2	2	2	2.140E7	45.6
Q5LFT7	Peptidase T OS	Bacteroides fragilis	89.56	5	1	1	1	7.323E7	45.5
A9NEA9	Serine hydroxymethyltransferase OS	Acholeplasma laidlawii	44.82	3	1	1	1	5.875E6	45.3
Q7MU77	Phosphoglycerate kinase OS	Porphyromonas gingivalis	54.70	1	1	1	1	2.106E7	45.0
Q8A753	Phosphoglycerate kinase OS	Bacteroides thetaiotaomicron	25.30	1	1	1	1	1.320E7	45.0
A5VHR0	Phosphopentomutase OS	Lactobacillus reuteri	159.08	1	4	4	4	4.364E7	44.0
A8EWM4	Phosphoglycerate kinase OS	Arcobacter butzleri	45.52	1	1	1	1	2.577E7	43.8
Q042T5	Elongation factor Tu OS	Lactobacillus gasseri	400.92	36	3	10	13	1.184E8	43.7
Q74JU6	Elongation factor Tu OS	Lactobacillus johnsonii	348.06	36	2	9	12	1.184E8	43.6
Q5L890	Elongation factor Tu OS	Bacteroides fragilis	185.88	297	3	5	7	1.454E8	43.6
Q8R603	Elongation factor Tu OS	Fusobacterium nucleatum subsp. nucleatum	150.02	302	1	3	3	6.170E7	43.4
B8J1A0	Elongation factor Tu OS	Desulfovibrio desulfuricans	139.50	64	2	3	3	4.287E7	43.4
A5VJ92	Elongation factor Tu OS	Lactobacillus reuteri	413.79	60	8	11	13	3.595E8	43.4

Note: *Score:* The Mascot score. Proteins: The total number of proteins contained in the protein group. *Unique Peptides:* The total number of peptides unique to the protein group. *Peptides:* The total number of peptides identified from all included searches for the master protein of the protein group. *PSMs:* The total number of peptide-spectrum matches identified from all included searches for the master protein of the protein group. *Area:* The chromatographic peak area was used to characterize the quantitative abundance of protein.*MW(kDa):* The theoretical molecular weight of the protein.

Table 3 Potential cross-reactive antigens identified in human fecal bacteria

NCBI Accession #	Protein Name	Bacterium	Score	Proteins	Unique Peptides	Peptides	PSMs	Area	MW [kDa]
A6LFK9	Polyribonucleotide nucleotidyltransferase OS	Parabacteroides distasonis	62.68	3	1	2	2	2.332E7	82.0
P75764	Uncharacterized protein YbhJ OS	Escherichia coli	27.35	1	1	1	1	3.198E7	81.5
Q8A4N6	Polyribonucleotide nucleotidyltransferase OS	Bacteroides thetaiotaomicron	226.97	23	6	7	7	6.947E7	78.3
B3DT30	Elongation factor G OS	Bifidobacterium longum	236.98	64	8	10	11	4.407E7	78.1
E1WNR6	Chaperone protein htpG OS	Bacteroides fragilis	131.15	4	1	2	2	4.992E7	77.9
O31673	ATP-dependent Clp protease ATP-binding subunit ClpE OS	Bacillus subtilis	120.19	73	1	3	4	8.448E7	77.9
A7ZSL5	Elongation factor G OS	Escherichia coli O139:H28	133.81	92	2	3	4	2.888E7	77.5
Q5L8A7	Elongation factor G OS	Bacteroides fragilis	431.35	187	3	10	14	1.391E8	77.5
A6KYJ7	Elongation factor G OS	Bacteroides vulgatus	361.61	186	2	9	12	1.342E8	77.4
A6LFP0	Methionine--tRNA ligase OS	Parabacteroides distasonis	65.86	8	1	1	1	4.772E7	77.4
P39396	Pyruvate/proton symporter BtsT OS	Escherichia coli	92.20	1	2	2	2	1.446E7	77.3
A9KNK6	Polyribonucleotide nucleotidyltransferase OS	Lachnoclostridium phytofermentans	68.87	1	1	1	1	1.075E8	76.9
Q5L6S5	Elongation factor G OS	Chlamydia abortus	76.05	58	1	2	3	1.622E7	76.8
Q67JU0	Elongation factor G OS	Symbiobacterium thermophilum	147.39	86	1	4	5	2.631E8	76.8
Q5U8S9	Elongation factor G OS	Staphylococcus intermedius	98.88	65	1	3	4	5.177E7	76.7
Q8A294	Putative K(+)-stimulated pyrophosphate-energized sodium pump OS	Bacteroides thetaiotaomicron	150.65	20	1	3	3	1.276E8	76.5
B9DYA6	Elongation factor G OS	Clostridium kluyveri	136.00	67	1	3	4	8.826E7	76.4
Q5WLR5	Elongation factor G OS	Bacillus clausii	134.85	81	1	4	5	1.119E8	76.4
Q97I51	Translation initiation factor IF-2 OS	Clostridium acetobutylicum	70.53	4	1	1	1	2.330E8	76.3
A0PXU3	Elongation factor G OS	Clostridium novyi	114.21	67	1	3	4	8.905E7	76.1
Q18CF4	Elongation factor G OS	Clostridioides difficile	174.49	59	1	4	5	1.288E8	75.8
Q8AB53	Putative glucosamine-6-phosphate deaminase-like protein BT_0258 OS	Bacteroides thetaiotaomicron	54.10	1	1	1	1	4.629E6	75.2
Q8XJ01	Penicillin-binding protein 1A OS	Clostridium perfringens	39.66	3	1	1	1	1.599E7	75.1
A6L7J7	Threonine--tRNA ligase OS	Bacteroides vulgatus	91.33	9	2	2	2	2.440E7	74.2
P30539	1,4-alpha-glucan branching enzyme GlgB OS	Butyrivibrio fibrisolvens	30.12	1	1	1	1	2.287E7	73.8
B2TIT5	Threonine--tRNA ligase OS	Clostridium botulinum	53.61	2	1	1	1	1.877E7	73.8

P56116	Chaperone protein HtpG OS	Helicobacter pylori	38.02	12	1	1	1	1.269E7	71.2
P0A9P7	ATP-dependent RNA helicase DeaD OS	Escherichia coli O6:H1	85.88	5	3	3	4	1.336E8	70.5
P19410	3-oxocholoyl-CoA 4-desaturase OS	Clostridium scindens	63.87	1	1	1	1	5.844E7	70.2
Q8RHJ2	Putative K(+)-stimulated pyrophosphate-energized sodium pump OS	Fusobacterium nucleatum subsp. nucleatum	140.41	23	1	3	3	1.320E8	68.9
A5CX56	Chaperone protein DnaK OS	Vesicomyosocius okutanii subsp. Calyptogena okutanii	15.38	1	1	1	1	2.961E7	68.7
Q5LG30	Chaperone protein DnaK OS	Bacteroides fragilis	418.39	33	1	9	11	6.399E7	68.6
Q89YW6	Chaperone protein DnaK OS	Bacteroides thetaiotaomicron	372.24	35	1	7	9	6.399E7	68.3
A6L2X7	Chaperone protein DnaK OS	Bacteroides vulgatus	371.71	33	1	8	10	6.399E7	68.3
Q93GF1	Chaperone protein DnaK OS	Prevotella loescheii	185.46	1	4	4	4	3.512E7	68.0
A6LGR5	4-hydroxy-3-methylbut-2-en-1-yl diphosphate synthase (flavodoxin) OS	Parabacteroides distasonis	38.34	5	1	1	1	2.396E7	67.9
B8H444	ATP-dependent zinc metalloprotease FtsH OS	Caulobacter vibrioides	26.45	6	1	1	1	1.241E7	67.7
A9KIA6	Aspartate--tRNA(Asp/Asn) ligase OS	Lachnoclostridium phytofermentans	31.12	1	1	1	1	8.400E6	67.5
P0AG91	Protein translocase subunit SecD OS	Escherichia coli O157:H7	233.70	2	6	6	6	2.164E7	66.6
Q49Y22	Chaperone protein DnaK OS	Staphylococcus saprophyticus subsp. saprophyticus	56.64	206	1	2	2	1.171E7	66.5
A6LBU6	Aspartate--tRNA ligase OS	Parabacteroides distasonis	88.06	49	1	2	2	7.901E6	66.4
P21332	Oligo-1,6-glucosidase OS	Bacillus cereus	53.99	2	1	1	1	1.391E7	66.0
Q8A5W4	Lysine--tRNA ligase OS	Bacteroides thetaiotaomicron	154.84	2	2	2	2	1.304E7	65.9
Q8GBW6	Methylmalonyl-CoA carboxyltransferase 12S subunit OS	Propionibacterium freudenreichii subsp. shermanii	98.01	1	1	1	2	1.386E8	65.9
Q67S54	Chaperone protein DnaK OS	Symbiobacterium thermophilum	96.29	225	1	3	3	4.528E7	65.7
Q9RQ13	L-fucose isomerase OS	Bacteroides thetaiotaomicron	181.20	7	1	5	7	1.038E8	65.7
A6L048	L-fucose isomerase OS	Bacteroides vulgatus	162.35	5	2	6	7	3.672E7	65.6
Q56403	V-type ATP synthase alpha chain OS	Thermus thermophilus	132.50	30	1	1	2	1.117E7	63.6
Q8G7I6	Glucose-6-phosphate isomerase OS	Bifidobacterium longum	531.07	4	14	14	15	3.155E8	63.0
Q4JX51	Glucose-6-phosphate isomerase OS	Corynebacterium jeikeium	30.85	1	1	1	1	3.306E7	62.1
Q8FZC4	2-isopropylmalate synthase OS	Brucella suis biovar 1	51.65	8	1	1	1	1.014E7	61.6
A6TGT4	Glucose-6-phosphate isomerase OS	Klebsiella pneumoniae subsp. pneumoniae	53.60	21	1	1	1	3.337E7	61.3

P0AG69	30S ribosomal protein S1 OS	Escherichia coli O157:H7	88.52	1	2	2	2	8.393E6	61.1
Q9EZ02	Pyrophosphate--fructose 6-phosphate 1-phosphotransferase OS	Spirochaeta thermophila	110.07	2	2	2	2	1.245E8	61.0
O31716	Uncharacterized ABC transporter ATP-binding protein YkpA OS	Bacillus subtilis	48.45	1	1	1	1	2.259E6	61.0
P59173	Probable 2,3-bisphosphoglycerate-independent phosphoglycerate mutase OS	Leptospira interrogans serogroup Icterohaemorrhagiae serovar Lai	61.50	2	1	1	2	6.104E6	61.0
P23843	Periplasmic oligopeptide-binding protein OS	Escherichia coli	368.94	2	11	11	12	1.586E8	60.9
Q0SQ82	Formate--tetrahydrofolate ligase OS	Clostridium perfringens	167.47	26	1	3	4	6.063E7	60.4
P14407	Fumarate hydratase class I, anaerobic OS	Escherichia coli	66.46	4	2	2	2	4.922E7	60.1
Q3A9K2	Formate--tetrahydrofolate ligase OS	Carboxydothermus hydrogenoformans	110.68	55	1	3	3	3.356E8	60.1
Q251P8	Formate--tetrahydrofolate ligase 1 OS	Desulfitobacterium hafniense	72.85	55	1	2	2	5.742E8	60.0
C0QX38	Formate--tetrahydrofolate ligase OS	Brachyspira hyodysenteriae	145.04	9	1	2	3	2.562E7	60.0
Q189R2	Formate--tetrahydrofolate ligase OS	Clostridioides difficile	157.46	1	3	3	3	1.347E9	59.9
C4ZBG8	Formate--tetrahydrofolate ligase OS	Agathobacter rectalis	235.86	56	4	6	6	3.610E8	59.7
A8AQV7	Phosphoenolpyruvate carboxykinase (ATP) OS	Citrobacter koseri	104.30	44	4	5	5	1.300E8	59.6
Q24ZZ8	Formate--tetrahydrofolate ligase 2 OS	Desulfitobacterium hafniense	79.67	55	1	2	2	5.193E8	59.4
B2RHV8	Phosphoenolpyruvate carboxykinase (ATP) OS	Porphyromonas gingivalis	188.39	21	2	5	5	2.446E8	59.4
Q47VD0	Phosphoenolpyruvate carboxykinase (ATP) OS	Colwellia psychrerythraea	111.53	16	1	2	2	1.952E8	59.3
A1R7X2	Arginine--tRNA ligase OS	Paenarthrobacter aurescens	43.93	15	1	1	1	2.994E7	59.2
Q8A414	Phosphoenolpyruvate carboxykinase (ATP) OS	Bacteroides thetaiotaomicron	293.03	21	3	8	8	3.939E8	59.1
C4ZBL1	Phosphoenolpyruvate carboxykinase (ATP) OS	Agathobacter rectalis	501.52	17	5	12	15	4.167E8	59.0
Q5L7N5	Phosphoenolpyruvate carboxykinase (ATP) OS	Bacteroides fragilis	420.91	17	1	6	12	2.103E8	59.0
A3CL27	Formate--tetrahydrofolate ligase 1 OS	Streptococcus sanguinis	145.32	20	1	2	3	3.296E7	59.0
A6LFQ4	Phosphoenolpyruvate carboxykinase (ATP) OS	Parabacteroides distasonis	438.19	17	5	11	14	2.336E8	58.9
C4ZAW6	Dihydroxy-acid dehydratase OS	Agathobacter rectalis	193.87	6	5	6	6	2.765E7	58.9
B9E299	Dihydroxy-acid dehydratase OS	Clostridium kluyveri	85.82	2	1	2	3	7.244E7	58.8
O09460	Phosphoenolpyruvate carboxykinase (ATP) OS	Anaerobiospirillum succiniciproducens	214.42	21	2	5	5	3.702E8	58.6
B2TIR2	Dihydroxy-acid dehydratase OS	Clostridium botulinum	46.21	2	1	1	1	3.131E6	58.5
B3DTV2	ATP synthase subunit alpha OS	Bifidobacterium longum	383.31	393	9	11	12	5.746E7	58.4
B3DRY6	Bifunctional purine biosynthesis protein PurH OS	Bifidobacterium longum	204.27	2	3	3	3	1.243E8	58.4
A6LIG0	60 kDa chaperonin OS	Parabacteroides distasonis	325.96	2	1	7	10	4.117E8	58.3

A5N857	Ribonuclease Y OS	Clostridium kluyveri	85.68	95	1	3	3	4.874E7	58.3
Q8G3N6	Inosine-5'-monophosphate dehydrogenase OS	Bifidobacterium longum	685.57	20	15	16	19	2.005E8	58.2
Q8A6P8	60 kDa chaperonin OS	Bacteroides thetaiotaomicron	591.81	1	2	11	15	2.794E8	58.2
Q5LAF6	60 kDa chaperonin OS	Bacteroides fragilis	690.75	1	4	15	20	5.301E8	58.2
A0Q2T1	60 kDa chaperonin OS	Clostridium novyi	58.42	6	2	2	2	2.212E8	58.1
A6KXA0	60 kDa chaperonin OS	Bacteroides vulgatus	948.24	1	11	22	26	6.146E8	58.1

Note: *Score:* The Mascot score. Proteins: The total number of proteins contained in the protein group. *Unique Peptides:* The total number of peptides unique to the protein group. *Peptides:* The total number of peptides identified from all included searches for the master protein of the protein group. *PSMs:* The total number of peptide-spectrum matches identified from all included searches for the master protein of the protein group. *Area:* The chromatographic peak area was used to characterize the quantitative abundance of protein. *MW(kDa):* The theoretical molecular weight of the protein.